1   Feeding in billfishes: inferring the role of the rostrum from a biomechanical standpoint

2

3

4   Habegger, M.L[1],*, Dean M.N[2], Dunlop, J.W.C.[2], Mullins, G[3], Stokes, M[3], Huber, D.R[4],Winters, D[3] and
5   Motta, P.J[1]

6
7
8   [1] Department of Integrative Biology
9   University of South Florida
10   4202 E. Fowler Ave
11   Tampa, FL 33613

12
13   [2] Department of Biomaterials
14   Max Planck Institute of Colloids & Interfaces
15   Am Muehlenberg 1
16   14476 Potsdam, Germany

17
18   [3] Department of Civil and Environmental Engineering
19   University of South Florida
20   4202 E. Fowler Ave
21   Tampa, FL 33613

22
23   [4] Department of Biology
24   University of Tampa
25   401 W. Kennedy Blvd
26   Tampa, FL 33606

27
28
29   [£] Corresponding author email: mhabegge@mail.usf.edu. (M.L Habegger)

30

31

32

33

34
35
36
37
38
39

40

41

42 Abstract

43   Perhaps the most striking feature of billfishes is the extreme elongation of the premaxillary bones

44 forming their rostra. Surprisingly, the exact role of this structure in feeding is still controversial. The goal

45 of this study is to investigate the use of the rostrum from a functional, biomechanical, and morphological

46 standpoint to ultimately infer its possible role during feeding. Using beam theory, experimental and

47 theoretical loading tests were performed on the rostra from two morphologically different billfish, the

48 blue marlin (*Makaira nigricans*) and the swordfish (*Xiphias gladius*). Two loading regimes were applied

49 (dorso-ventral and lateral) to simulate possible striking behaviors. Histological samples and material

50 properties of the rostra were obtained along their lengths to further characterize structure and mechanical

51 performance. Intraspecific results show similar stress distributions for most regions of the rostra,

52 suggesting this structure may be designed to withstand continuous loadings with no particular region of

53 stress concentration. Although material stiffness increased distally, flexural stiffness increased proximally

54 owing to higher second moment of area. The blue marlin rostrum was stiffer and resisted considerably

55 higher loads for both loading planes as compared to that of the swordfish. However, when a continuous

56 load along the rostrum was considered, simulating the rostrum swinging through the water, swordfish

57 exhibited lower stress and drag during lateral loading. Our combined results suggest the swordfish

58 rostrum is suited for lateral swiping to incapacitate their prey, whereas the blue marlin rostrum is better

59 suited to strike prey from a wider variety of directions.

60

61 **Introduction**

62   The billfishes (marlins, spearfishes, sailfishes and swordfish) are large and fast pelagic predators

63 characterized by the extreme elongation of their upper jaw bones to form an elongated rostrum, or bill

64 (Nakamura, 1985, Davie, 1990, Fierstine, 1990, Fierstine and Voigt, 1996). Surprisingly the function of

65 this structure is still controversial (Nakamura, 1983, Frazier et al., 1994). The rostrum has been

66   hypothesized to improve hydrodynamics by reducing drag (Wisner, 1958, Ovchinnikov, 1970; Aleyev,

67   1977; but see Sagong, et al. 2014), to be used for defense (as evidenced by rostral fragments found

68   embedded in large predators; Fierstine, 1997; Fierstine et. al., 1997), and to be used to strike, immobilize

69   or dismember prey before ingestion, thereby facilitating feeding (Gudger, 1940, Talbot and Penrith, 1964,

70   Scott and Tibbo, 1968). Although it is certainly possible that the elongated rostrum may have been

71   selected for multiple roles, substantial evidence from stomach contents, and recent field observations

72   strongly support the latter feeding-related hypothesis (Scott and Tibbo, 1968; Stillwell and Kohler, 1985,

73   Frazier et al., 1994, Shimose et al., 2007, Domenici et al., 2014).

74   The geometries and relative sizes of the rostra of different billfish species are in some cases

75   strikingly different, suggesting the use of the rostrum in feeding is perhaps species-specific. The rostrum

76   of swordfish (the only species within the Xiphiidae), which can exceed 50% of body length, is wide,

77   distally tapered, and dorsoventrally flattened with a lenticular cross-section, having sharp edges, and

78   lacking teeth (Gregory and Conrad, 1937; Gudger, 1940; Poplin et al., 1976; Nakamura, 1983; Fierstine,

79   1990; Fierstine and Voigt, 1996; Nohara et al., 2003). Conversely, in istiophorids (marlins, spearfishes

80   and sailfishes), the rostrum is more circular in cross-section, has no sharp edges, and is surrounded by

81   small villiform teeth. The length of the rostrum varies among species but is proportionally shorter than in

82   swordfishes, being approximately 24% of body length in blue marlin (Gudger, 1940, Nakamura, 1983).

83   These structural differences between swordfish and marlin are indeed reflected in anecdotal accounts of

84   feeding events, where swordfish are suggested to slash their prey with only lateral movements of the

85   rostrum (Scott and Tibbo, 1968, McGowan, 1988), and istiophorids are described as stunning and/or

86   spearing their prey, thereby using a wider range of rostral movements (Talbot and Penrith, 1964;

87   Fierstine, 1997; Fierstine et al., 1997; Shimose et al., 2007). Correlations of these differences in rostral

88   form and behavior between species, and their mechanical implications at the tissue level have, however,

89   been nearly impossible to study due to the logistical issues associated with the study of large, fast, pelagic

90   predators such as billfishes (but see Domenici et al., 2014).

91   Biomechanical approaches offer feasible ways to investigate the potentially differing roles of the

92   rostrum in the various billfish species, enabling the quantification of mechanical performance and

93   facilitating the inference of behavior from morphology. The utility of these approaches has been

94   demonstrated for experimentally intractable taxa, via investigations of feeding mechanics in white sharks,

95   bull sharks and rorqual whales (Wroe et al., 2008; Field et al., 2011; Habegger et al., 2012). Significant

96   advances in biomechanical studies have been accomplished through the utilization of beam theory, an

97   engineering approach that describes the mechanical behavior of a beam under loading. This approach is

98   applicable because many biological structures can be treated as beams (e.g. trees, echinoderms, vertebral

99   columns) (Koehl, 1977; Baumiller, 1993; Ennos, 1993; Huber et al., 2013), and beam theory also

100   facilitates better comprehension of form and function relationships by allowing the teasing apart of factors

101   that contribute to a biological beam's performance under loading. A beam's resistance to bending is given

102   by the flexural stiffness, EI, which is a function of both its material properties (via Young's modulus, E)

103   and its geometry (via second moment of area, I) (Koehl, 1976; 1977; Wainwright et al., 1976; Biewener,

104   1992). Analyses of a structure's cross-sectional geometry and the response of its material to load (e.g. the

105   force per unit area, or stress, σ, that builds in a material under load in response to deformation, or strain,

106   ε) can therefore provide an understanding of the overall structure's mechanical capabilities and limits,

107   with stress distributions and yield behavior pointing to performance boundaries, all of which can offer

108   clues to loading regimes likely experienced *in vivo*. As EI accounts for both material and structural

109   properties, it is a useful metric for characterizing mechanical function in comparative studies, particularly

110   when linking organismal function with evolutionary and ecological pressures (Koehl, 1976; 1977;

111   Macleod, 1980; Etnier, 2003). Flexural stiffness has been shown to correlate with loading regime and

112   direction for a range of biological body support systems, from the limb skeletons of batoids and dogs, to

113   the jaws of whales and pelicans, to the exoskeletons of crabs (Kemp et al., 2005; Taylor et al., 2007; Field

114   et al., 2011; Macesic and Summers, 2012); these taxonomic comparisons also illustrate that higher levels

115   of bending resistance can be attained evolutionarily by either increases in E, I or both.

116   The goal of this study is to use biomechanical models and material testing to infer the possible

117   biological role(s) of the rostrum in two billfish species with differing rostrum morphologies, the blue

118   marlin (*Makaira nigricans,* Lacepede, 1802) and the swordfish (*Xiphias gladius,* Linnaeus, 1758).

119   Utilizing beam theory as our primary model, we estimate several biomechanical variables and describe

120   the material properties and geometric attributes of the rostrum along its length in order to acquire a better

121   understanding of its function and mechanical capabilities. Inferences of the putative feeding behaviors of

122   these two apex predators are then made based on these analyses, paying special attention to suggestions of

123   how mechanical and growth demands may be balanced for these biological cantilevers. Since failure or

124   large deflections could be detrimental during feeding we hypothesize that stress will be equally

125   distributed along the length of the rostrum, preventing any localized region of higher stress ("weak

126   spots") that could lead to failure during feeding. Correspondingly, we expect flexural stiffness to be

127   uniform along the length of the rostrum and sufficiently large to avoid appreciable deflections while

128   striking prey. Based on previous descriptions of cross-sectional geometry, we expect that the swordfish

129   rostrum will be better suited for lateral striking of prey, whereas that of the blue marlin will be suited for a

130   larger range of motions.

131   Results

132   *Histology*

133   The rostra of both species are composed of similar tissue types that appear to be arranged in

134   similar patterns along the length of the rostra (Fig. 1, 2). Three main tissues were observed: acellular bone

135   (a bone lacking osteocytes, Cohen et al., 2012), adipose tissue, and hyaline cartilage, with proportions of

136   the tissues changing in distinct ways from tip to base. The primary component of distal cross-sections

137   (Fig. 1A-D, Fig. 2A-D) was acellular bone. Moving proximally towards the base of the rostrum, adipose

138   tissue and hyaline cartilage become more dominant, particularly in area 4, where they comprise most of

139   the center of the cross-section (Fig. 1E, F, Fig. 2 E, F) and acellular bone is relegated to the periphery.

140   Although the majority of the adipose tissue was found in area 4, this tissue was also observed

141   intermittently in smaller quantities within canals present throughout the acellular bone of the rostrum.

142   *Geometric analysis*

143   Swordfish and blue marlin exhibited diagnostic differences for most of the variables in our CT-

144   scan based analysis of cross-sectional geometry, indicating that the observed species-specific

145   morphologies have mechanical consequences. Second moment of area (I, a descriptor of the cross-

146   sectional distribution of material in the direction of loading and a proxy for bending resistance) increased

147   proximally in both species and in both principle loading directions, particularly at ~75-80% bill length

148   (BL), where the rostrum begins to merge with the head region. However, the ratio of I for loading in the

149   dorsoventral and lateral directions ($Imaj/Imin$) differed considerably between species, as a function of the

150   dissimilar cross-sectional shapes of the species' rostra. Swordfish rostra are extremely asymmetric in

151   morphology and in the contribution of rostrum shape to bending resistance, with I in lateral bending ~10-

152   16 times greater than that for dorsoventral bending. This ratio is greatest distally and decreases proximally

153   as the rostrum deepens closer to the head (Fig. 3A). In blue marlin I was only slightly greater for loading

154   in the lateral direction, and the ratio of $Imaj/Imin$ was fairly constant along the length of the rostrum (~2-

155   3), indicating a more uniform distribution of material and isotropic bending resistance (Fig. 3B; Table 1).

156   In proximal regions of the rostrum, bone forms only a thin peripheral layer but is arranged far

157   from the neutral axis, resulting in a high I for a comparatively small amount of bone tissue. This is

158   reflected in the abrupt proximal (~ 75-80% BL) decrease in the proportion of mineralized tissue in each

159   cross-section (Figs. 3C, D), as well as in our histological data, which show a proximal decrease in bone

160   and increase in adipose tissue and cartilage (Figs. 1-2). Whereas in blue marlin the proportion of

161   mineralized tissue in cross-sections is approximately 100% in distal sections (< ~80% BL), representing a

162   solid bony rostrum, in swordfish the proportion of mineralized tissue shows jagged oscillation distally,

163   reflecting the periodic bony chambers within the distal rostrum (Fig. 3C). Both species show a proximal-

164 to-distal increase in the mean relative bone mineral density of the rostra, whereas the pattern of decrease

165 in swordfish is more gradual, and that of blue marlin is consistent until approximately 70% BL and then

166 decreases more sharply (Figs. 3C, D).

167 *Bending experiments in a material testing system (MTS)*

168 Stresses along the rostrum were calculated as a function of rostral geometry and load during

169 bending experiments where rostra tips were displaced +/-1cm. Although the magnitude of stresses in the

170 rostra of the two species were considerably different, with blue marlin stresses being two to four times

171 higher, both species showed an approximately similar distal-to-proximal trend of slight increase in stress

172 from area 1 to 2 and then a gradual decrease to area 4. During lateral loading, the average maximum

173 stress distribution did not vary much along the swordfish rostrum, ranging from 1.4 to 1.6 N/mm^2 (areas

174 1-4 respectively). During dorsoventral loading, the stress distribution was higher along the rostrum

175 ranging from 2.1 to 1.3 N/mm^2 (areas 1-4 respectively, Fig. 4A, Table A1). For the blue marlin, the

176 average maximum stress distribution during lateral loading ranged from 7.8 to 3.9 N/mm^2 (areas 1-4

177 respectively) with stress in the three most distal areas being considerably greater than that in the most

178 proximal section (area 4). Similarly, during dorsoventral loading, the stress distribution in the three distal

179 areas ranged from 8.7 to 9.2 N/mm^2, and area 4 decreased to 4.9 N/mm^2 (Fig. 4B, Table A1).

180 In the swordfish, Young's modulus, E, decreased proximally from 12.2 to 5.3 GPa when

181 calculated in lateral loading (areas 1-4 respectively), and from 12.9 to 3.1 GPa when calculated in

182 dorsoventral loading (Fig. 4C, Table A1). Although similar trends in E were observed for the blue marlin,

183 values tended to be larger, ranging from 14.5 to 3.5 GPa in lateral loading and from 16.4 to 5.7 GPa in

184 dorsoventral loading (Fig. 4D, Table A1).

185 Flexural stiffness, which accounts for both material and geometric contributions to bending

186 resistance, increased proximally in the swordfish during lateral (3.7×10^5 to 9.6×10^5 $GPa\ mm^4$) and

187 dorsoventral loading ($2.9\ 10^4$ to $1.2\ 10^5$ $GPa\ mm^4$) (Fig. 4E). Flexural stiffness also increased proximally

188 in the blue marlin, although values between the two loading planes were more similar than those of the

189   swordfish, especially for the distal half of the rostrum. During lateral loading *EI* ranged from $4.2\ 10^5$ to

190    $2.0\ 10^6$ GPa mm^4 and dorsoventrally from $2.4\ \text{x}10^5$ to $1.3\ \text{x}\ 10^6$ GPa mm^4 (Fig. 4F). (For the full range of

191   values see appendix 1)

192   It took considerably larger loads to displace the blue marlin rostrum the same fixed distance (±1

193   cm) as that of the swordfish (maximum loads applied to the blue marlin rostrum were 173.0 N and 123.9

194   N compared to the swordfish 19.3 N and 7.1 N, lateral and dorsoventral loading, respectively). Therefore,

195   rather than comparing stresses resulting from both species' maximum loads, we determined the largest

196   moment value during the swordfish experiments, and then for each strain gauge, determined the

197   corresponding stresses resulting from a similar moment value in both blue marlin specimens. This

198   "standardized" stress allowed us to illustrate the difference in the species' tissue stress responses to the

199   same moment, as opposed to the responses to the same maximum displacement. The use of the swordfish

200   maximum moment as a reference value for both species was preferred over load standardizations

201   (standardizing the values to similar loads for each species) to account for small differences in the position

202   of the strain gauges between species because bending moment calculations take into account both load

203   and distance from load. Results from standardized moments showed similar stress values for both species

204   during lateral loading with the exception of area 4 for blue marlin, which was considerably lower.

205   However, during dorsoventral loading, swordfish rostra showed almost three times greater stresses (Table

206   2, Fig. 5A, B).

207

208   *Biological loading scenarios: Point loading and hydrodynamic loading*

209   For a hypothetical point loading scenario, swordfish had higher stress values along the rostrum in

210   both loading planes compared to blue marlin (Fig. 6A). Stresses calculated for the swordfish rostrum

211   during dorsoventral loading were considerably larger than those for lateral loading, diminishing towards

212   the base (Fig. 6A). Stress values for blue marlin were lower and very similar for both loading planes.

213   Simulations of hydrodynamic loading during head swinging indicated that swordfish experience the

214   highest maximum stress and drag during dorsoventral loading and lowest maximum stress and drag

215   during lateral loading, with blue marlin values being intermediate for both variables in both loading

216   directions(Fig. 6B, C).

217   **Discussion**

218   Our data suggest that the morphological differences observed between swordfish and blue marlin

219   rostra have performance implications, and that these morphological and mechanical differences may be

220   consistent with different feeding behaviors. Considering the possible role of the rostrum during feeding,

221   the blue marlin rostrum is built like a short, solid javelin with cross-sectional anatomy suggesting multi-

222   axial use; in contrast, the swordfish rostrum appears suited for use as a light-weight, low drag, uniaxial

223   weapon.

224   Despite the cross-sectional shape differences between the two species, our data show several

225   material and structural commonalities between blue marlin and swordfish rostra, providing strong

226   evidence that common evolutionary pressures (e.g. growth, use in feeding) may have shaped rostral

227   anatomy in both species. In general, both rostra show opposing trends in I and E, with the former

228   increasing rapidly proximally, but the latter increasing distally (Fig. 4C, D). The decrease in E proximally

229   means that the increase in EI must solely result from disproportionate changes in I. The distribution of

230   grayscale intensity in rostrum CT scans suggests that bone mineral density increases distally in the

231   rostrum in both species (Fig. 3C, D), perhaps explaining the observed stiffness gradient, as E and mineral

232   density are positively associated in a variety of mineralized tissues (Currey, 2004; Horton and Summers,

233   2009; Magwene and Socha, 2013).

234   Stress values in the tissue resulting from the bending experiments were shown to be

235   approximately similar among the distal regions (areas 1-3) for both species (Fig. 4A, B). A strategy to

236   keep stress constant along the length of a cantilever beam is to increase the cross-sectional area towards

237   the fixed end, compensating for the increase in bending moment (Currey, 1984). Billfish rostral cross-

238   sectional area and I increase proximally (Figs. 1-3), likely explaining the consistent stresses in the distal

239   regions. Stress values tended to be comparatively low in area 4, achievable due to the comparatively large

240   *I* values at the base (>60% bill length). This increase in *I* is a function of the change in geometry and the

241   large cross-sectional areas in proximal regions, but also the peripheral arrangement of bone in this area.

242   This arrangement allows for a high *I* without necessitating increased weight, as the core of the base of the

243   rostrum is filled with low density materials (adipose tissue and cartilage) that are lighter than a

244   comparable rostrum of solid bone (Fig. 1, Fig. 2, area 4). Biological structures that have a similar

245   conformation (solid exterior and a softer, light-weight interior) such as the toucan beak, porcupine quills,

246   and feather shafts (Bonser, 2001; Seki, et al. 2005; Meyers, 2013) have been suggested to not only

247   increase *I* in a structure but also to decrease the probability of local buckling by dissipating fracture

248   energy and preventing the collapse of the thin cortical walls, while also minimizing weight (Ma et al.,

249   2008; Meyers, 2013). Furthermore, Gudger (1940) proposed this filling in billfishes may also act as shock

250   absorber, dampening vibrations during striking of prey.

251   The ecological implications of the distal increase in material stiffness may be associated with

252   feeding, as this change minimizes deflection of the distal portion of the rostrum and provides a hard

253   surface for striking prey. Billfish rostra are subject to periodic loadings over long periods of time, which

254   may result in fatigue damage and favor the formation of microcracks in this stiffer area, as in bone and

255   nacre (Currey, 1984). Similar gradients of stiffness have been reported in other biological structures

256   including bird feathers (Macleod, 1980; Bonser and Purslow, 1995), squid beaks (Miserez et al., 2009)

257   and spider fangs (Politi et al., 2012), the latter two systems also acting as predatory weapon, similar to

258   billfish rostra . In addition, the higher incidence of remodeled bone morphology in the distal region of the

259   rostrum, suggest the tissue is under regular loading and therefore more prone to damage and

260   consequently, remodeling (Atkins et al., 2014). Distal stiffening of rostral material could also counteract

261   structural tapering relating to hydrodynamic demands. Previous work has shown that the drag experienced

262   during lateral swiping of the elongate rostrum in alligators is proportional to the height of the jaws

263   (McHenry et al., 2006). Minimizing element height (via distal tapering) may reduce drag in billfish rostra,

264   however it also comes at the cost of potentially reducing cross-sectional area and resistance to bending

265 (McHenry et al., 2006); distal stiffening of the rostrum may ultimately be a strategy for maintaining

266 adequate flexural stiffness in areas where I is selected to be comparatively low for hydrodynamic reasons.

267 Additionally, since the bow wave generated by a predator can be detected by prey (Visser, 2001), the

268 relatively smooth and elongated rostrum of billfishes may reduce water disturbance, thereby delaying

269 detection of approaching billfish by prey, as suggested for other vertebrates with long jaws including

270 water snakes and alligators (Alfaro, 2002; McHenry et al, 2006).

271   Generalized patterns of stress, material stiffness, second moment of area, and flexural stiffness in

272 both billfish rostra seem to follow a common pattern that may aid in overcoming conflicting demands

273 imposed by the rostrum's function and shape. Evidence from the histology and mineral density gradient

274 of the rostrum found in this study, in addition to that in an ongoing investigation of billfish tissue

275 morphology (Atkins et al., 2014), indicate that distal regions of the billfish rostrum are less porous, more

276 mineral dense, and more remodeled. This suggests that distal areas may contain older tissue than basal

277 regions and therefore that the rostrum in billfishes may grow from its base by "pushing" older material

278 distally (although rostrum development is not fully understood and other factors such as mechanical

279 demands may play a role in its development). We have shown that basal regions of the rostrum (i.e.

280 suggested growth zones) are prone to less stress and, due to the proximal increase in I, EI was also

281 increased. The lower values of stress at the base of rostrum also coincide with a region of multiple

282 sutures, where multiple cranial bones converge, and where the rostrum connects to the rest of the head

283 (Fig. 7). Sutures have been found to influence patterns of stress and strain by resisting or allowing

284 deformations depending on load orientation and/or magnitude (Rafferty et al., 2003; Markey et al., 2006;

285 Krauss et al., 2009) but also can act as bone deposition sites in mammals (Opperman, 2000; Sun et al.,

286 2004) and so may provide free surfaces for growth and bone deposition in billfish rostra. All of these

287 factors may decrease the likelihood of failure at this region, preventing the compromise of vital organs

288 such as the nares, and also preventing damage to a region of higher vascularization and growth.

289 Coincidentally, rostra in several different billfish species have been more often documented to show

290 breaks in their distal halves (Frazier et al., 1994; Fierstine and Crimment, 1996; Fierstine et. al. 1997).

291   Although broad structural similarities clearly exist between rostra of these species, their

292   morphological differences revealed mechanical disparities that suggest different feeding behaviors.

293   While I was approximately equal for both species during lateral loading (Fig. 3A, B), the blue marlin

294   rostrum showed higher I during dorsoventral loading and greater equivalence of bending resistance

295   between lateral and dorsoventral loading ($I_{maj}/ I_{min} \sim 1.0$) due to its almost circular cross-section, as

296   compared to the swordfish ($I_{maj}/ I_{min} > 8.0$) (Fig. 3A, B). Additionally, blue marlin rostra showed E values

297   higher than those for swordfish for most of the regions along the rostrum (Fig. 4C, D) and E varied with

298   respect to loading regime in swordfish, suggesting material heterogeneity in this species. Overall, stiffness

299   values calculated from distal strain gauge data (area 1, 12.9 GPa swordfish and 16.4 GPa blue marlin)

300   agree with those determined in a different study for five billfish species (including those studied here)

301   using material testing techniques (E ranged between 12-20 GPa; Atkins et al., 2014) but also exceed the

302   values found in other acellular boned fishes, such as great sculpin, *Myoxocephalus polyacanthocephalus*

303   (6.48 GPa; Horton and Summers, 2009) and tilapia *Oreochromis aureus* (7.20 GPa; Cohen et al., 2012) as

304   well as those with cellular bone found in the common carp, *Cyprinus carpio* (8.51 GPa; Cohen et al.,

305   2012). Moreover values of stiffness in billfish are not only shown to be higher than most values reported

306   for other fish but also to be closer to values reported for mammals (Atkins et al., 2014).

307   Mechanical demands associated with feeding may not be the only factors dictating shape

308   differences between species. Drag forces, for example, are influenced by a structure's shape, surface

309   characteristics, speed of movement, and the surrounding fluid's density and viscosity (Vogel, 2003), and

310   therefore drag forces acting on the rostra can conceivably influence feeding. Our results from modeled

311   biological loading scenarios indicate that drag force and stress during dorsoventral loading are greater in

312   swordfish than blue marlin. Swordfish rostra, however, would exhibit the lowest drag force during lateral

313   loading (Fig. 6C) due to the depressed lenticular form of the rostrum. Consequently swordfish may be

314   limited in the extent to which they can use dorsoventral striking, which incurs 40-times the drag forces

315   compared to lateral striking (Fig. 6C). Interestingly, this support for differences in rostrum motion during

316   striking are also suggested by differences in vertebral morphology between the two species. The vertebral

317   column of the blue marlin is reinforced with zygapophyses that provide reinforcement and stability but

318   decrease flexibility (Hebrank et al., 1990). In contrast, the lack of zygapophyses in swordfish may allow

319   extensive lateral flexibility of their body, as Hebrank et al. (1990) found that the flexibility of the blue

320   marlin vertebral column increased when the zygaphophyses were removed. The potentially greater lateral

321   flexibility of the swordfish body may be related to the dorsoventral depression of the rostrum and its

322   reduced hydrodynamic drag in the horizontal plane, facilitating low-resistance, lateral swiping at its prey.

323   Patterns of σ, *E*, *I*, *EI* and theoretical drag calculations suggest that blue marlin may have a

324   rostrum better suited to strike its prey in a wider range of motions, similar to the multi-plane striking

325   behavior observed during feeding in sailfish (Domenici et al., 2014), a species with a rostrum similar in

326   shape to that of the blue marlin. Rod-like structures are suited to withstand loading in multiple directions,

327   whereas elliptical cross-sectional beams, such as the swordfish rostrum, are better designed to withstand

328   loading in a single plane (Etnier and Vogel, 2000, Currey, 2002). Injuries to prey provide insight into

329   billfish feeding behavior (Scott and Tibbo, 1968, Nakamura, 1985, Stillwell and Kohler, 1985). Prey

330   fishes in the stomach contents of blue marlin showing lacerations to the dorsal, ventral, and caudal body

331   regions (Shimose, 2007) and pictures of sailfish prey bearing injury on differing regions of the body (Fig.

332   8A) support our theory of multi-directional striking in istiophorids. In contrast, gut contents of swordfish

333   showed prey being severed which may be due to the lateral swiping of the sharp, lenticular rostrum of

334   (Goode, 1883; Stillwell and Kohler, 1985) (Fig. 8B).

335   In conclusion, blue marlin rostra are stiffer and better suited to strike prey in multiple planes,

336   whereas swordfish rostra seem to be highly specialized for lateral striking due to the arrangement of

337   skeletal material in a way that maximizes lateral bending resistance while decreasing drag. However,

338   despite the differences found between these species there are still many variables converging into similar

339   patterns that may explain how to build an efficient biological beam that can act as a weapon in multiple

340   ways. Whether this structure evolved as an adaptation for feeding remains uncertain, but its design, tissue

341   architecture, and material properties favor its role in prey capture.

Material and methods

342

343   Four swordfish (*Xiphias gladius*) and two blue marlin heads (*Makaira nigricans*) (Table 3) with

344   intact rostra were obtained from fishing tournaments in the Gulf of Mexico, USA. Heads were transported

345   to the University of South Florida and frozen with the rostrum wrapped in plastic to reduce dehydration.

346   After being thawed all heads were CT scanned with a 64 slice Aquilon Toshiba scanner Toshiba

347   American Medical Systems Inc., Tustin, CA, USA with slice thickness ranging from 0.75-1.0 mm (image

348   size 512x512 pixels, pixel size 0.625 mm). After scans were completed, samples were wrapped in plastic

349   bags and kept frozen until material testing. Whole skull scans were rendered for figure purposes using

350   Mimics software (Materialise HQ, Belgium). The use of all tissue samples was approved under the

351   University of South Florida Institutional Animal Care and Use Committee, IACUC protocol number T

352   3884.

353   *Histology*

354   In order to investigate the tissues comprising the rostra, transverse sections were prepared for

355   both swordfish (n=1) and blue marlin (n=1) at four regions along each rostrum, mirroring the locations of

356   strain gauge placement (see bending experiment section). Four transverse sections (areas 1-4, distal to

357   proximal) of approximately one half-centimeter thickness were cut from one representative rostrum of

358   each species. Transverse sections were preserved in 10 % buffered formalin followed by decalcification

359   in formic acid (50 % HCOOH, 50 % H_2O) -sodium citrate (500 g $NaH_2C_6H_5O_7$, 2500 ml H_2O). Sections of

360   4 µm were made with a Bioacut microtome (Leica/Reichert Jung model 2030, Wetzlar, Germany) and

361   stained using hematoxylin and eosin. Samples were observed under compound microscope (Leica CTR

362   6500 Wetzlar, Germany). Pictures were taken at two magnifications, 50 and 100x, with a digital camera

363   (Leica DFC 420c Wetzlar, Germany). Although this tissue had been subjected to previous freeze-thaw

364   cycles, which may compromise bone tissue and cellular ultrastructure (e.g. nuclei and osteocytes;

365 Andrade et al., 2008), these changes are irrelevant for the scale of our observations and osteocytes are

366 lacking from the bone of these species.

Geometric analysis

368 In order to understand geometric/structural contributions to the mechanical performance of

369 billfish rostra, we applied beam theory analyses to transverse sections of the rostra of 4 swordfish and 2

370 blue marlins (Table 3) using a custom MATLAB script described below. Our analyses were restricted to

371 the contribution of hard tissue (bone) as CT scanning captures only bone structure accurately and bone

372 occupies the majority of the rostra.

373 Rostral bone was isolated within each dataset using the Segmentation Editor in Amira (Mercury

374 Computer Systems, Berlin, Germany) by first digitally isolating the rostrum (by cropping out all tissue

375 caudal to the nares). The rostrum includes a range of tissue types (e.g. bone, cartilage, adipose tissue); to

376 extract the bony tissue, we selected the largest peak from the scan's histogram distribution of grayscale

377 values, and then made small-scale adjustments to the selection range while noting the effect on the

378 morphological accuracy of the resultant volume (i.e. whether the volume represented more or less bone

379 than was known from dissection to be there). This "bone selection" method resulted in more

380 morphologically accurate volumes than an alternate method, where the grayscale thresholding range was

381 set at the start of the MATLAB script through an iterative series of threshold steps on individual original

382 (full grayscale range) CT slices. However, when thresholding methods were compared for the same CT

383 datasets, analyses of cross-sectional geometry in MATLAB (see below) produced nearly identical trends,

384 indicating the technique is robust, regardless of thresholding method.

385 Each resultant thresholded (i.e. "bone-only") volume was sectioned orthogonal to the longitudinal

386 axis of the rostrum and an image stack of cross-sections exported to the MATLAB script. The script then

387 performed a slice-wise analysis of cross-sectional geometry, beginning by normalizing rostrocaudal

388 positions to percent lengths to facilitate comparison across scans (i.e. the slice containing the rostral tip

389 represented 0% length, the slice containing the caudal end of the rostrum represented 100% length).

390   Slices were then selected at intervals of 2% element length; this selection interval was determined via

391   sensitivity analysis to provide a balance of resolution of data trends and script efficiency.

392   For each of the 51 slices per rostrum, the script converted the grayscale "bone-only" images to

393   binary images (white = bone; black = soft tissue and voids) and analyzed the distribution of white pixels

394   around the cross-section's centroid in order to determine a series of variables describing rostrum cross-

395   section geometry: second moment of area, I; cross-sectional area, (A); and filled-CSA (A_f; the area of the

396   element cross-section with any holes/internal black pixels converted to white pixels) (Fig. 9).

397   Second moment of area describes the distribution of material around a neutral axis (NA) in a

398   cross-section and perpendicular to the line of applied force, and is therefore indicative of resistance to

399   bending. Billfish rostra contain multiple tissues with different material properties, which can be

400   accounted for by scaling the contribution of each tissue according to its Young's modulus (Gere, 2002).

401   However, as the non-bony tissues are located closer to the NA and their moduli are as of yet unknown

402   (although likely orders of magnitude less), we simplify the analysis by focusing only on the bone tissue

403   and assuming it has a consistent modulus down the length of the rostrum and between species.

404   The second moments of area of any shape around a given axis is given by $I=\int y^2 \, dA$, where y is

405   the perpendicular distance of the area element dA from that axis. For simple shapes this is readily

406   calculated analytically and tables of appropriate formula can be found in textbooks. For complex shapes

407   where no easy analytical equation is available, it is possible to divide the complex shape up into simple

408   shapes for which the second moment of area is known, and add these values together weighted by the

409   distance of the centroids of each shape to the bending axis (Gere 2002). We apply this approach to the

410   complex geometries of our CT data, so that for each cross section, the second moment of area about a

411   given neutral axis (NA) is calculated with the following equation:

$$I_{NA} = \sum_{}^{n} (I_{pix} + A_{pix} \, y^2) \qquad (1)$$

412   where n is the number of individual pixels; I_{pix} is the second moment of area of each pixel relative to its

413   own centroid, $(a^4)/12$; A_{pix} is the pixel area, a^2, where a = 0.625mm; y is the perpendicular distance from

414   the NA (NA was determined as the axis perpendicular to the applied force passing through the centroid

415   of each cross section). Apart from the term (I_{pix}) in the summation, this equation is identical to the

416   standard integral; the I_{pix} term, however, is important when there are few pixels in an examined cross-

417   section and/or y is small compared to the pixel size (i.e. at the extreme proximal or distal ends of the

418   rostra), as the area of each pixel is proportionately more important to the cross-section's second moment

419   of area. For large and/or thick-walled cross-sections, when y is large compared to the pixel size, the

420   corrective term I_{pix} would be negligible and our equation and the standard integral would effectively yield

421   the same results.

422   However, as the second moment of area of asymmetrical sections can vary with the chosen

423   bending axis —evidenced by the example of an architectural I-beam with a higher second moment of area

424   when bent in line with its longer cross-sectional axis— we calculated second moment of area for bending

425   in line with the major axis (I_{maj}) and the bending in line with the minor axis (I_{min}) of each cross-section.

426   The major and minor axes are defined as the longest and shortest diameters of the cross-section; in both

427   species, these structural axes correspond to the lateromedial and dorsoventral axes of the rostra,

428   respectively (see cross-sections in Fig. 9). The ratio of the two moments (I_{maj}/I_{min}) is a mechanical aspect

429   ratio, describing the anisotropy of bending resistance for the cross-section. Whereas an ellipse would

430   exhibit a higher ratio, indicating a greater resistance to bending along one axis, a circle's moment ratio

431   would be 1.0, indicating isotropy in bending resistance.

432   We further described the cross-sectional distribution of material by calculating the proportion of

433   bone (number of white pixels, A) per cross-section relative to that of the hypothetical filled cross-section

434   (A_f):

$$\%Min = A/A_f \qquad (2)$$

435   In addition the relative mineral content per cross-section was estimated by calculating the average

436   grayscale value of mineralized tissue. As the scans were not calibrated to materials of known mineral

437   density (e.g. using imaging phantoms of varying hydroxyapatite composition), these values are only

438   meaningful as relative measurements and so are presented as percentages of each scan's maximum value,

439   from 0-100%.

Bending experiments in a material testing system (MTS)

441   Billfish heads were thawed and prepared for material testing by removing all soft tissues from the

442   skull. Once cleaned, each skull (neurocranium) was potted in fast curing cement (Rockite, Hartline

443   products, Cleveland, OH, USA), firmly encasing the head while leaving the entire rostrum exposed,

444   simulating a cantilever beam. The embedded skull was then anchored to the floor via a holding device

445   (Fig. 10) and the tip of the rostrum fixed to the crosshead of a materials testing device by a custom made

446   wooden clamp that enveloped the rostrum cross section allowing vertical motion and load dispersal along

447   the cross section. The attachment point of the MTS was located approximately 15% of the rostrum length

448   from the tip, representing a loading point (LP) that might be expected during prey contact. To determine

449   the reaction of tissue along the length of the rostrum to distal loads, four transverse regions were

450   demarcated (areas 1 through 4, distal to proximal), starting at 30% rostrum length and spaced

451   approximately 20% apart. The criteria for the selection of these points were based on the relative

452   positions that represented the best locations to survey strain along the majority of the rostrum accounting

453   for differences in length in both species. Each area was fitted with six strain gauges oriented parallel to

454   the longitudinal axes of the rostrum (C2A-13-125LW-120, Vishay Measurements Group, Inc. Raleigh,

455   NC, USA): four on the dorsal surface (two lateral and two medial) and two on the medial ventral surface

456   (Fig. 10). For proper strain gauge attachment, each region was smoothed with 400-grade sandpaper, and

457   excess oil removed with acetone. Strain gauges were glued to the underlying bone with Mbond glue

458   (Vishay Measurements Group, Inc. Raleigh, NC, USA). Because some of the skeletal elements at the base

459   of the most proximal portion of the rostrum in blue marlin (area 4) are supported medially by soft tissue,

460   and removing them could greatly affect the structural integrity of the rostrum, strain gauges could not be

461   attached here, decreasing the total number of strain gauges for this species to 22.

462   Because the location of the NA depends on load orientation, different strain gauges were selected

463   for the two different loading regimes utilized (lateral and dorsoventral). For example, only strain gauges

464   located on the lateral edges of the rostrum were analyzed during lateral loading (Fig. 10). Due to the lack

465   of knowledge of rostral bending during normal feeding behaviors in billfish and the limitations of our

466   MTS system, displacements were fixed to ±1 cm for all bending tests. Each rostrum was loaded under

467   displacement control at the same loading point with a 50 lb load cell (JP 50, Honeywell, Golden Valley,

468   MN, USA) at a frequency of 2 Hz in a material testing system, this was the maximum frequency allowed

469   by our system, since higher values resulted in vibration interference (MTS System Corporation,

470   Minneapolis, MN, USA). Loading tests were conducted in dorsoventral and lateral planes to simulate

471   likely striking directions, with data (strains, cross-head displacement and measured force) recorded at

472   1000 Hz in a Megadac data collection system (Optim electronics corporation Germantown, MD, USA)

473   Using beam theory the following variables were estimated for each of the four areas on each

474   rostrum. Stress was calculated using the following equation,

$$\sigma = My/I \quad (3)$$

475   where M is the bending moment at each area calculated by multiplying the maximum measured load from

476   each bending regime by the distance from the loading point to each position where most strain gauges

477   were aligned for each area; at a given position, d, y is the in-plane distance from the NA to each strain

478   gauge at that location (Fig. 10); and I is the second moment of area associated to each NA (mm^4). For

479   each area's cross-section, I and y were calculated in MATLAB; for the latter, physical measurements of

480   the distances of strain gauges from the lateral edge of the rostrum were used to determine their

481   dorsoventral positions in each digital cross-section, and the dorsoventral distance y of those points from

482   the neutral axis. Since we were interested in estimating the maximum stress generated by the rostrum

483   during a set displacement, stress was calculated utilizing the largest bending moment at each area for each

484   experiment (made by the product of the largest load and the distance from the strain gauges at each area

485   to the loading point). Although the stress formula has been formulated based on simple structures in

486   engineering, it has been widely used in biological systems, however, caution should be taken at

487   interpreting its results since some deviation from its original assumptions may apply (i.e. the rostra don't

488   have a constant cross sectional area).

489   Using the stress calculated above, Young's modulus was calculated to estimate the material

490   stiffness at each strain gauge location using the following equation:

$$E = \sigma / \varepsilon \quad (4)$$

491   where $\square$ is the strain gathered from strain gauges at the maximum bending moment. Estimating E by this

492   method assumes that the material is linearly elastic, however, similar values of E, derived from the slope

493   of stress-strain curves, were estimated from three-point bending experiments on the same billfish species

494   by Atkins et al. (2014), supporting our results. Flexural stiffness (GPa*mm^4) was calculated:

$$Flexural\ stiffness = E \times I \quad (5)$$

495   where E is Young's modulus and I is the second moment of area previously calculated. This parameter

496   estimates the resistance to bending of the rostrum at all areas, allowing an integrated understanding of

497   material properties and responses to load along the length of the rostrum.

498   *Biological loading scenarios: Point loading and hydrodynamic loading*

499   In addition to the geometric analyses above, we used a second MATLAB script to examine the

500   effects of cross-sectional form on rostral stresses for both species for two possible loading conditions:

501   point-loading (a single/point load, equivalent to the billfish striking a prey item with the tip of the

502   rostrum) and hydrodynamic loading (a load along the full length of the rostrum, resulting from the

503   rostrum being swiped through the water) (Fig. 11). (see Appendix 2 for complete methods).

504   **Author contribution**

505   Designed and implemented experiments: MLH. Designed and implemented geometrical analyses and

506   biological loading simulations: MND, JD. Contributed to data acquisition and analysis: MLH, MND, DH,

Table 1. Second moment of area obtained from MATLAB geometrical analysis along the rostrum of two billfish species, swordfish (*X. gladius*) and blue marlin (*M. nigricans*)

	Second moment of area (mm^4)			
	Area 1	Area 2	Area 3	Area 4
SWF $_{LAT}$	27241	56466	104200	168425
SWF $_{DV}$	2243	5537	10939	37397
BM $_{LAT}$	29797	48747	104991	603445
BM $_{DV}$	15139	25917	57228	224365

Second moment of area at four regions along the rostrum (area 1- area 4) for swordfish (SWF) and blue marlin (BM) during lateral (LAT) and dorsoventral (DV) bending

Table 2. Standardized values of stress obtained from bending experiments in blue marlin (*M. nigricans*).

	Standarized Stress (N/mm^2)			
	Area 1	Area 2	Area 3	Area 4
SWF $_{LAT}$	1.4 ± 0.2	1.7 ± 0.3	1.6 ± 0.3	1.6 ± 0.3
SWF $_{DV}$	2.1 ± 0.2	2.1 ± 0.2	2.0 ± 0.2	1.3 ± 0.2
BM $_{LAT}$	1.3 ± 0.2	1.9 ± 0.2	1.7 ± 0.3	0.7 ± 0.3
BM $_{DV}$	0.7 ± 0.1	1.0 ± 0.1	0.8 ± 0.0	0.4 ± 0.0

Standardized stress values in blue marlin (BM) along the rostrum (mean ± SE areas 1 and 4 respectively) during lateral (LAT) and dorsoventral (DV) bending. Values of stress in swordfish are the same as in table

Table 3. Specimen information. Meristic data from both species utilized in this study swordfish (*X. gladius*) and blue marlin (*M. nigricans*)

Species	Lj-FL (cm)	Weight (Kg)	BL(cm)
X. gladius (SFW)	125	36.1	72.4
X. gladius (SFW)	138.7	38.2	77.5
X. gladius (SFW)	146.1	39.9	77.5
X. gladius (SFW)	147.3	37.7	78
M. nigricans (BM)	257	172.5	59.5
M. nigricans (BM)	257.8	147.1	61.7

Total length estimations in billfishes are commonly measured as lower jaw- fork length (Lj-FL), bill length was measured as the distance from the tip to the naris and is denoted as (BL)

Figure legends

Fig. 1. Results from histological analysis performed along four regions of the rostrum of a swordfish. Top image from left to right shows representative cross-sections from areas 1 to 4. Images **A-D** show acellular bone present in all regions. Images **E** and **F** show different tissues found on area 4 including cartilage and adipose tissue. Cross-section orientation: dorsal on top, ventral on bottom. Upper surface of cross-section is the dorsal portion of the rostrum, nc = nutrient canals.

Fig. 2. Results from histological analysis performed along four regions of the rostrum of a blue marlin. Top image from left to right shows representative cross-sections from areas 1 to 4. Images **A-D** show acellular bone present in all regions (white areas around the edge of the rostrum in **B** and **C** show no tissue). Images **E** and **F** show different tissues found on area 4 such as cartilage and adipose tissue. Cross-section orientation: dorsal on top, ventral on bottom. Upper surface of cross-section is the dorsal portion of the rostrum, nc = nutrient canals.

Fig. 3. Results from geometrical analysis along the length of the rostrum (0 % = distal tip, 100 % = proximal base) of swordfish (right column, mean ± SE, n=4) and blue marlin (left column, mean ± SE, n=2). **A, B** show second moment of area (I, mm^4) blue lines show I about the dorsoventral plane (I_{min}) and red lines show I about the lateral plane (I_{maj}), green lines show the ratio between second moments of area (I_{maj}/I_{min}). **C, D** show, down the length of the rostrum, the percent of cross-sectional area occupied by bone tissue (% mineralization) (blue lines) and the relative bone tissue grayscale values (a proxy for bone mineral density, calculated relative to each CT scan's maximum; red lines).

Fig. 4. Intraspecific results from bending experiments in two loading planes (mean ± SE, swordfish values on the left and blue marlin on the right). **A, B,** stress distribution along the rostrum (N/mm^2). **C, D**, Young's modulus (GPa). **E, F**, flexural stiffness (GPa*mm^4). Black and white circles denote different loading orientations (black, lateral load) and (white dorsoventral load).

Fig. 5. Interspecific comparisons of standardized stress (N/mm^2) from bending experiment in two loading planes **A**, lateral plane and **B,** dorso-ventral plane (mean ± SE). Standardizations were performed in blue marlins (white circles) while swordfish values (black circles) where not modified.

Fig. 6. Comparisons of localized and continuous loads among species and loading orientations. **A**, Stress applied at a localized point. **B**, load continuously applied along the rostrum. **C**, drag forces along the rostrum. Each color represents a species with a particular loading plane, blue lines are swordfish loaded laterally, red lines swordfish loaded dorsoventrally, green lines blue marlin loaded laterally and purple lines blue marlin loaded dorsoventrally. Rostrum length goes from 0 (most distal part) to 700 most proximal portion.

Fig. 7. CT scan reconstruction of a swordfish rostrum. Bones are individually labeled and colored; the locations of the strain gauges are marked in area 4 to illustrate their arrangement in this highly sutured area on the proximal portion of the rostrum. Bone nomenclature follows Fierstine and Voigt (2006), however, the prenasal bone is still controversial for this species and is demarked with an question mark (see Fierstine, 1990)

Fig. 8. **A.** Injuries in prey items after a sailfish (*Istiophorus albicans*) feeding event in Isla Mujeres, Mexico. Arrows denote possible multiplane points of impact from the rostrum (*Pers. Comm*. Rafael de la Parra). B. Decapitated squid from stomach contents of a swordfish suggesting possible lateral slashing used during feeding behavior (*Pers. Comm*. Eduard Walker). Since in both cases direct feeding events were not documented other types of feeding behavior may be equally viable.

Fig. 9. Illustration of the cross-sectional shape differences between species and description of the major steps performed during the MATLAB geometric analysis. From top to bottom: complete skull renderings for both species (swordfish left and blue marlin right) followed by grayscale "bone-only" thresholded rostrum sections utilized for the analysis (number of cross-sections shown were reduced for space purposes), followed by binary images (black and white). Binomial images were produced every 2% along

the rostrum and the ratio of bending moments between two loading planes (*Imaj/Imin*), among other variables, were calculated and graphed along the rostrum.

Fig. 10. Outline of the apparatus settings for the bending experiments on the material testing system (MTS) during lateral loading on a swordfish rostrum. Strain gauge (SG) location and areas along the rostrum are shown on the dorsal portion of the rostrum (from the most distal area, area 1 to the most proximal, area 4). The complete layout of strain gauges can be observed within the dashed box showing a magnified representative cross-section of area 2. Some representative examples of variables utilized for the calculation of stress are shown where *d* represents the distance from the loading point to the area in question (in the figure, this is area 1) and *y* represents the distance from the neutral axis (NA) to one strain gauge on the dorsal surface of the cross-section. Note that although the calculation of *d* and *y* are shown here for only one strain gauge in area 1, these variables were calculated in each area (1-4).

Fig. 11. Simulated point load vs. hydrodynamic load scenarios in a swordfish with dorsal and lateral views of suggested loading regimes. A similar loading simulation was conducted for the blue marlin. **A** shows a point load simulating a lateral and dorsoventral load exerted by a prey item at the most distal portion of the rostrum (red arrow). **B** simulates the effect of water exerting a continuous load along the length of the rostrum (blue arrows) during lateral and dorsoventral movement of the head.

References

Andrade M. G. S., Sa, C. N., Marchionni, A. M. T., de Bittencourt, T. C. B. do. S. C. and Sadigursky, M. (2008). Effects of freezing on bone histological morphology. *Cell Tiss. Bank.* **9**, 279-287

Aleyev, Y. G. (1977). *Nekton*. Junk, The Hague.

Alfaro, M. E. (2002). Forward attack modes of aquatic feeding water snakes. *Func. Ecol.* **16**, 204-215

Atkins, A., Dean M.N., Habegger M.L., Motta, P.J., Ofer, L., Repp, F., Weiner, S., Currey, J., Shahar, R. (2014). Remodeling of anosteocytic bone. Proc. Nat. Acad. Sci. 111:16047-16052.

Baumiller, T. K. (1993). Crinoid stalks as cantilever beams and the nature of the stalk ligament. *Neues Jahrb. Geol. Palaeontol. Abh.* **190,** 279-297.

Biewener, A. A. and Full, R. J. (1992). *Biomechanics Structures and Systems: A Practical Approach*, ed. Biewener, A. A. Oxford Univ. Press, Oxford.

Bonser, R. H. (2001). The mechanical performance of medullary foam from feathers. *J. Mat. Sci. Let.* **20**, 941-942.

Cohen, L., Dean, M., Shipov, A., Atkins, A., Monsonego-Ornan, E. and Shahar, R. (2012). Comparison of structural, architectural and mechanical aspects of cellular and acellular bone in two teleost fish. *J. Exp. Biol.* **215**, 1983-1993.

Currey, J. D. (1984). The mechanical adaptations of bone. Princeton, NJ: Princeton University Press.

Currey, J. D. (2002). *Bones: Structure and Mechanics.* Princeton, NJ: Princeton University Press.

Currey, J. D. (2004). Incompatible mechanical properties in compact bone. *J. Theor. Biol*. **231**, 569-580

Davie, P. (1990). *Pacific Marlins: Anatomy and Physiology*. Palmerston North, New Zealand Massey Univ. Press.

Denny, M. (1993). *Air and Water: The Biology and Physics of Life's Media*. Princeton, NJ: Princeton Univ. Press.

Dill, L. M. (1974a). The escape response of zebra danio (*Brachydanio rerio*). The stimulus for escape. *Anim. Behav.* **22**, 710-721.

Domenici, P., Wilson, A.D.M., Kurvers, R.H.J.M., Marras, S., Herbert-Read, J.E., Steffensen, S., Krause, S., Viblanc, P. E., Couillaud, P. and Krause, J. (2014). How sailfish use their bills to capture schooling prey. Proc. Roy. Soc. **281**. http://dx.doi.org/10.1098/rspb.2014.0444.

Ennos, A. R. (1993). The mechanics of the flower stem of the sedge *Carex acutiformis. Ann. Bot.* **72**, 123-127.

Etnier, S. E. and Vogel, S. (2000). Reorientation of daffodil (Narcissus: Amaryllidacea) flowers in wind: drag reduction and torsional flexibility. *Am. J. Bot.* **87**, 29-32.

Etnier, S. E. (2003). Twisting and bending of biological beams: distribution of biological beams in a stiffness mechanospace. *Biol. Bull.* **205**, 36-46.

Field, D. J., Lin, S. C., Ben-Zvi, M., Goldbogen, J. A., Shadwick, R. E. (2011). Convergent evolution driven by similar feeding mechanics in balaenopterid whales and pelicans. *Anat. Rec: Adv. Integ. Anat. Evol. Biol..* **294**, 1273-1282.

Fierstine, H. L. (1974). The paleontology of billfish-the state of the art. Proceedings of the International Billfish Symposium, Kailua-Kona, Hawaii, 9-12 August 1972. Part 2. Review and contributed papers. NOAA Technical Report NMFS SSRF-675 pp. 34-44.

Fierstine, H. L. (1990). A paleontological review of three billfish families (Istiophoridae, Xiphiidae and Xiphiorhynchidae). Pages 11–19 *in* R. H. Stroud, ed. Planning the future of billfishes. Part 2. Contributed papers. Proc. 2nd Int. Billfish Symposium, Kailua-Kona, Hawaii, August 1-5, 1988.

Fierstine, H. L. and Crimmen, O. (1996). Two erroneous, commonly cited examples of "swordfish" piercing wooden ships. *Copeia.* **1996**, 472-475.

Fierstine, H. L. and Voigt, N. L. (1996). Use of rostral characters for identifying adult billfishes (Teleostei: Perciformes: Istiophoridae and Xiphiidae). *Copeia* **1996**, 148-161.

Fierstine, H. L. (1990). A paleontological review of three billfish families (Istiophoridae, Xiphiidae, and Xiphiorhynchidae). Pages 11–19 *in* R. H. Stroud, ed. Planning the future of billfishes. Part 2. Contributed papers. Proc. 2nd Int. Billfish Symp., Kailua-Kona, Hawaii, August 1-5, 1988.

Fierstine, H. L. (1997). An Atlantic Blue Marlin, *Makaira nigricans*, impaled by two species of billfishes (Teleostei: Istiophoridae). *Bull. Mar. Sci.* **61**, 495-499.

Fierstine, H. L., Cailliet, G. M. and Neer, J. A. (1997). Shortfin Mako, *Isurus oxyrinchus*, impaled by blue marlin, *Makaira nigricans* (Teleostei: Istiophoridae). *Bull. South. Calif. Acad. Sci*. **3**, 117-121.

Frazier, J. G, Fierstine, H. L., Beavers, S. C., Achaval, F., Hiroyuki, S., Pitman, R. L., Yamaguchi, Y. and Prigioni, C. M. (1994). Impalement of marine turtles (Reptilia, Chelonia: Cheloniidae and Dermochelyidae) by billfishes (Osteichthyes, Perciformes: Istiophoridae and Xiphiidae). *Env. Biol. Fish*. **39**, 85-96.

Gere, J. M. (2002). *Mechanics of Materials*. 5 Ed. Stamford, CT: Brooks/Cole Publishing Co.

Gudger, E. W. (1940). The allegated pugnacity of the swordfish and the spearfishes as shown by their attacks on vessels. *Roy. Asiatic. Soc., Bengal Branch, Mem.* **2**, 215-31.

Habegger, M.L., Motta, P.J., Huber, D.R., Dean, M.N. (2012). Feeding biomechanics and theoretical calculations of bite force in bull sharks (*Carcharhinus leucas*) during ontogeny. *Zoology***115**, 354-364

Hebrank, J. H., Hebrank, M. R., Long, J. H., JR, Block, B. A. and Wainwright, S. A. (1990). Backbone mechanics of the blue marlin *Makaira nigricans* (Pisces, Istiophoridae). *J. Exp. Biol*. **148**, 449-459.

Hoerner, S. F. (1965). *Fluid-Dynamic Drag*. Hoerner Fluid Dynamics: Brick Town, NJ.

Horton, J. M., and Summers, A. P. (2009). The material properties of acellular bone in a teleost fish. *J. Exp. Biol*. **212**, 1413-1420.

Huber, D. R., Neveu, D. E., Stinson, C. M., Anderson, P. A. and Berzins, I. K. (2013). Mechanical properties of sand tiger (*Carcharias taurus*) vertebrae in relation to spinal deformity. *J. Exp. Biol*. **216**, 4256-4263.

Koehl, M. A. R. (1976). Mechanical design in sea anemones. In: *Coelenterate Ecology and Behavior* (ed G.O. Mackie). Plenum Publishing Corp.

Koehl, M. A. R. (1977). Mechanical organization of cantilever like sessile organism: sea anemonies. *J. Exp Biol.* **6**, 127-142.

Nakamura, I. (1983). Systematics of the billfishes (Xiphiidae and Istiophoridae). *Publ. Seto Mar. Biol. Lab.* **28**, 255-396.

Nakamura, I. (1985). *Billfishes of the world*. FAO Species Catalogue. FAO Fish. Synop. No.125, vol. 5, 1-65.

Nohara, K., Hiroshi, O., Motoki, N., Kazuhiko, H., Nobuaki, S., Makoto, O. and Chow, S. (2003). Biological investigation on two types of bill internal structure of swordfish (*Xiphias gladius*) and genetic differentiation between the North and South Atlantic stocks. *Bull. Fish. Res. Agen*. **7**, 1-13.

Ma, J., Chen, W., Zhao, L. and Zhao, D. (2008). Elastic buckling of bionic cylindrical shells based on bamboo. *J. Bion. Eng*. **5**, 231-238

Macesic, L. J. and Summers, A.P. (2012). Flexural stiffness and composition of the batoid propterygium as predictors of punting ability. *J. Exp. Biol*. **215**, 2003-2012.

Macleod, G.D. (1980). Mechanical properties of contour feathers. *J. Exp. Biol*. **87**, 65-71.

Magwene, P. M. and Socha, J. J. (2013). Biomechanics of turtle shells: how whole shells fail in compression. *J. Exp. Zool*. **319**, 86-98.

Markey, M. J, Main, R. P and Marshall, C. R. (2006). In vivo cranial suture function and suture morphology in the extant fish *Polypterus*: implications for inferring skull function in living and fossil fish. *J. Exp. Biol.* **209**, 2085-2102.

Meyers, M. A., McKittrick, J. and Chen, P. (2013). Structural biological materials: critical mechanics-materials connections. *Science* **339**, 773-779

McGowan, C. (1988). Differential development of the rostrum and mandible of the swordfish (*Xiphias gladius*) during ontogeny and its possible functional significance. *Can. J. Zool*. **66**, 496-503.

McHenry, C. R., Clausen, P. D., Daniel, W. J. T., Meers, M. B. and Pendharkar, A. (2006). The biomechanics of the rostrum in crocodilians: a comparative analysis using finite element modeling. *Anat. Rec*. **288,** 827-849.

McHenry, M. J., Claverie, T., Rosario, M. V. and Patek, S. N. (2012). Gearing for speed slows the predatory strike of a mantis shrimp. *J. Exp. Biol.* **215**, 1231-45.

Miserez, A., Schneberk, T., Chengjum, S., Zok, F. W. and Herbertwaite, J. (2009). The transition from stiff to compliant materials in squid beaks. *Science*. **319**, 1816-181.9

Opperman, L. A. (2000) Cranial sutures as intramembranous bone growth sites. *Dev. Dyn*. **219**, 472-485.

Ovchinnikov, V. V. (1970). Swordfish and billfishes in the Atlantic Ocean. Ecology and functional morphology. Isr. Prog. Sci. Trans. NOAA NMFS TT 71-50011.

Politi, Y., Priewasser, M., Pippel, E., Zaslansky, P., Hartmann, J., Siegel, S., Li, C., Barth, F. G., and Fratzl, P. (2012). A spider's fang: How to design an injection needle using chitin‐based composite material. *Adv. Func. Mat.* **22**, 2519-2528.

Poplin, C., Poplin, F. and Rieqles, A. (1976). Quelques particularités anatomiques et histologiques du rostre de l'espadon *(Xiphias gladius* L.). *C. R. Acad. Sci. Ser. D.* **282**, 1105-1108.

Rafferty, K. L, Herring, S. W and Marshall, C. D. (2003). Biomechanics of the rostrum and the role of facial sutures. *J. Morph.* **44**, 257-233.

Rho, J. Y., Mishra, S. R., Chung, K., Bai, J. and Pharr, G. M. (2001). Relationship between ultrastructure and nanoindentation properties of intramuscular herring bones. *Ann. Biomed. Eng*. **29**, 1082-1088.

Sagong, W., Jeon, W-P., Choi, H. (2013). Hydrodynamic characteristics of the sailfish (*Istiophorus platypterus*) and swordfish (*Xiphias gladius*) in gliding postures at their cruise speeds. PLoS ONE **8**, e81323. doi:10.1371/journal.pone.0081323.

Seki, Y., Schneider, M. S. and Meyers M. A. (2005). Structure and mechanical properties of the toucan beak. *Acta Mat.* **53**, 5281-5296.

Scott, W. B. and Tibbo, S. N. (1968). Food and feeding habits of swordfish, *Xiphias gladius*, in the Western North Atlantic. *J. Fish. Res. Bd. Canada.* **25**, 903-972.

Shimose, T., Yokawa, K., Saito, M. and Tachihara, K. (2007). Evidence for the use of the bill by blue marlin (*Makaira nigricans*), during feeding. *Ichtyol. Res*. **54**, 420-422.

Shimose, T., Yokawa, K., Saito, M. and Tachihara, K. (2008). Seasonal occurrence and feeding habits of black marlin (*Istiompax indica*), around Yonaguni Island, southwestern Japan. *Ichthyol. Res*. **55**, 90-94.

Stillwell, C. E. and Kohler, N. E. (1985). Food and feeding ecology of the swordfish *Xiphias gladius* in the western North Atlantic Ocean with estimates of daily ration. *Mar. Ecol.* **22**, 239-247.

Sun, Z., Lee, E., Herring, S. (2004). Cranial sutures and bones: growth and fusion in relation to masticatory strain. *Anat. Rec. Part A* **276**, 150-161.

Talbot, F. H. and Penrih, J. J. (1964). Spearing behavior in feeding in the black marlin, *Istioampax marlina*. *Copeia* **1964**, 468.

Van Der Elst, R. P. and Roxburgh, M. (1981). Use of the bill during feeding in the black marlin (*Makaira indica*). *Copeia* **1981**, 215.

Visser, A. W. (2001). Hydromechanical signals in the plankton. *Mar. Ecol. Prog. Ser*. **222**, 1-24

Vogel, S. (2003). *Comparative Biomechanics: Life's Physical World*. Princeton: Princeton University Press.

Wainwright, S. A., Biggs, W. D., Currey, J. D. and Gosline, J. M. (1976). *Mechanical Design in Organisms*. Princeton, NJ. Princeton Univ. Press.

Wisner, R. (1958). Is the spear of istiophorid fishes used in feeding? *Pac. Sci*. **12**, 60-70.

Wroe, S., Huber, D. R., Lowry, M., McHenry, C., Moreno, K., Clausen, P., Ferrara, T., Cunningham, E., Dean, M. N. and Summers, A. P. (2008). Three-dimensional computer analysis of white shark jaw mechanics: how hard can a great white bite? *J. Zool.* **276**, 336-342.
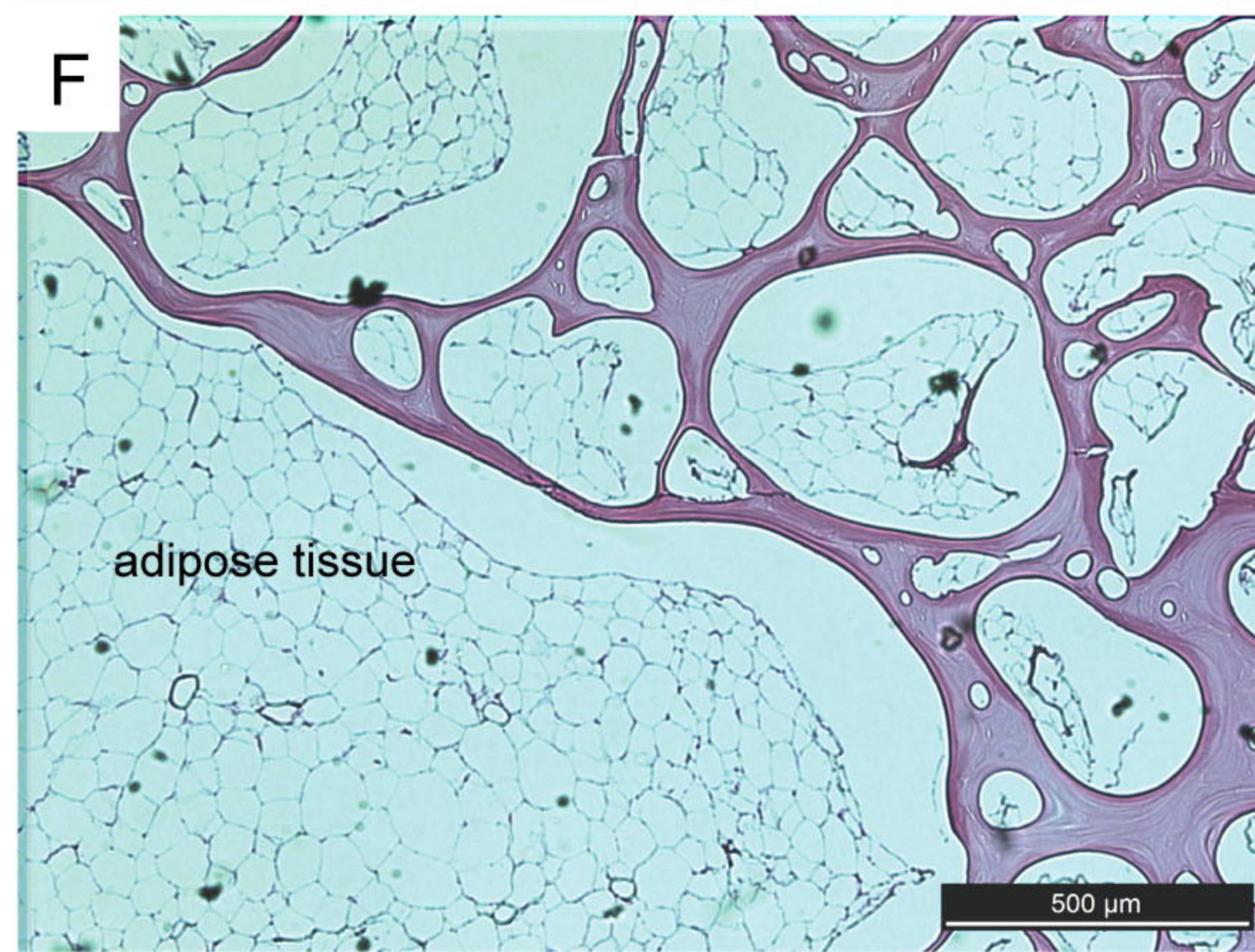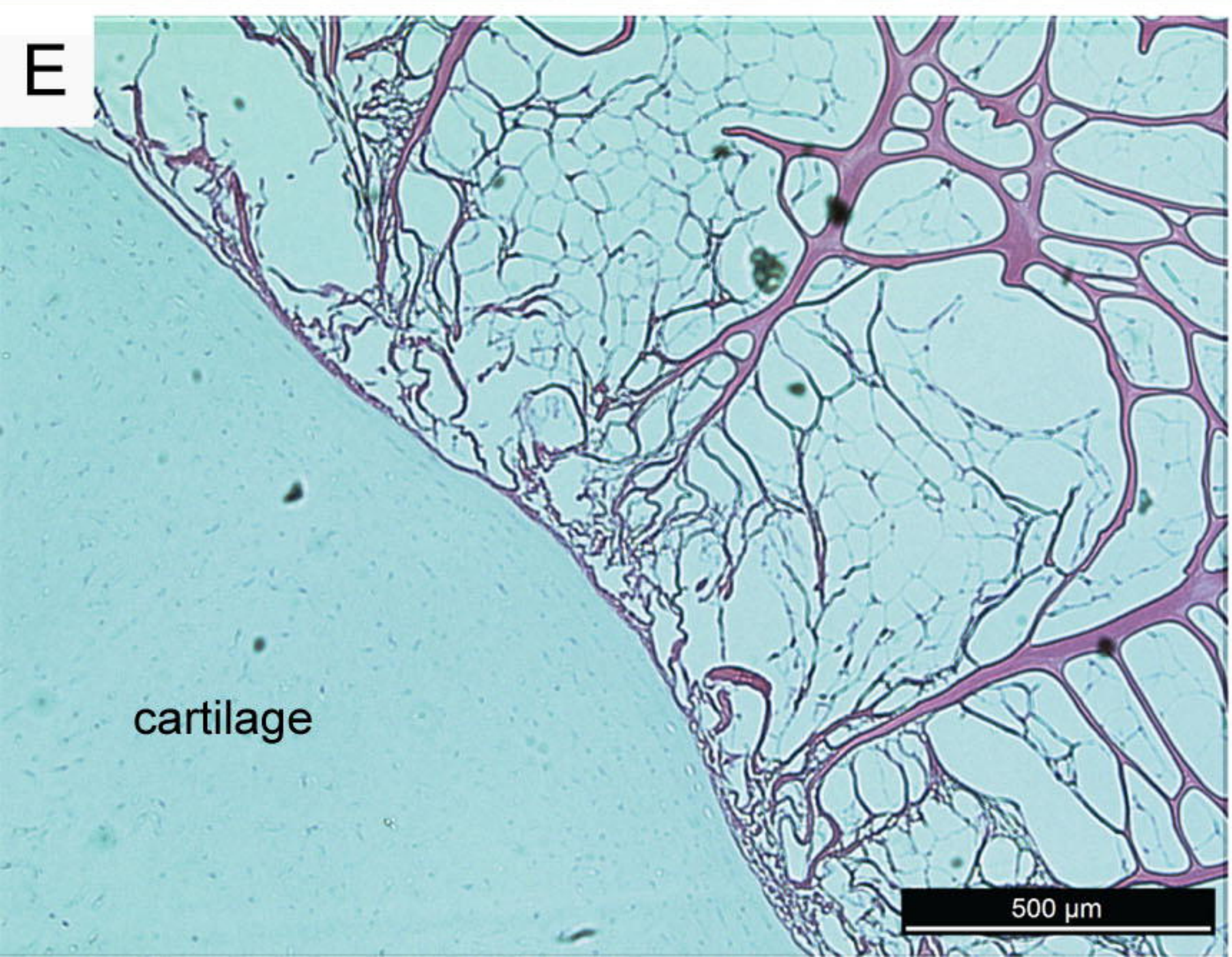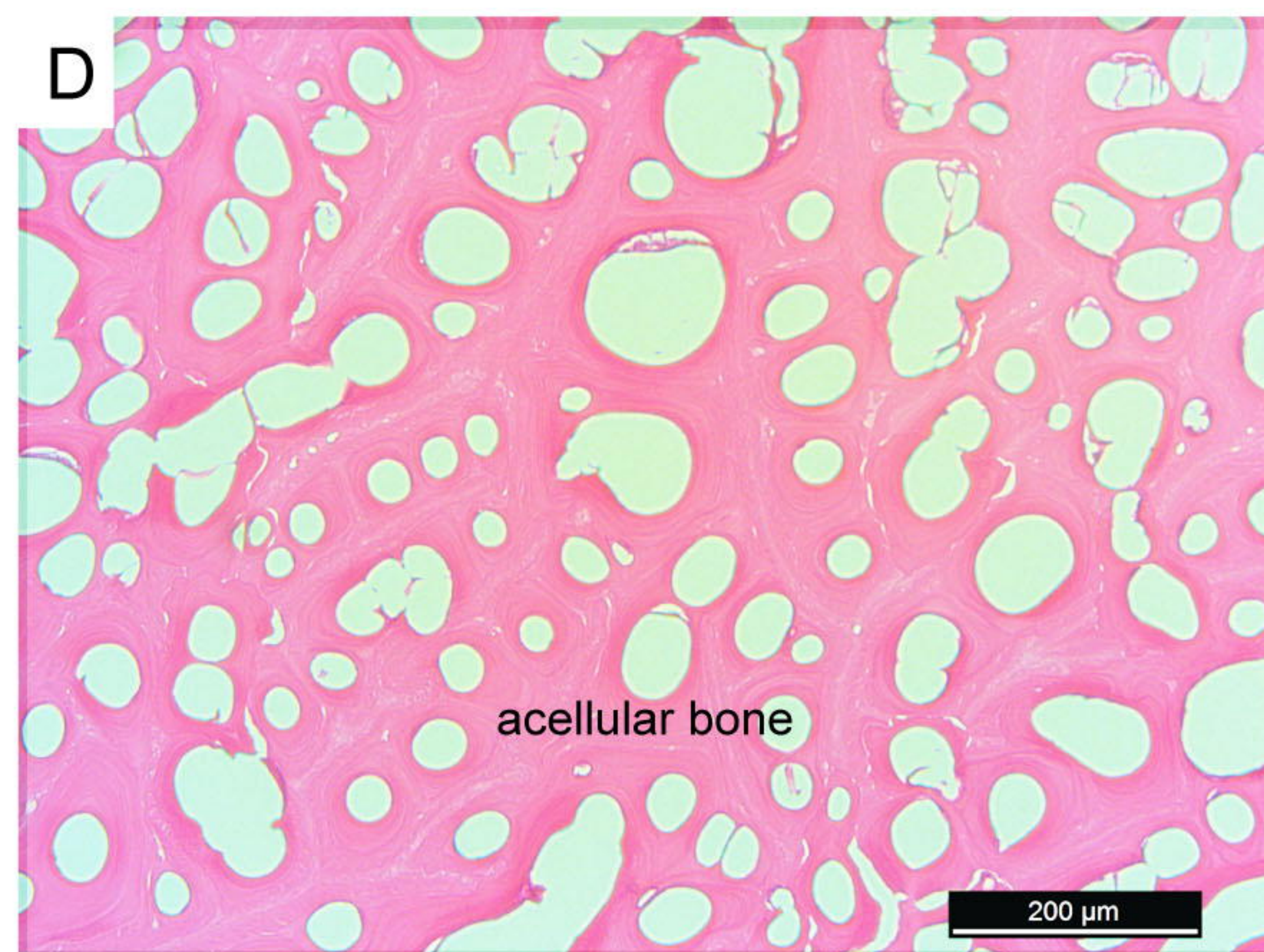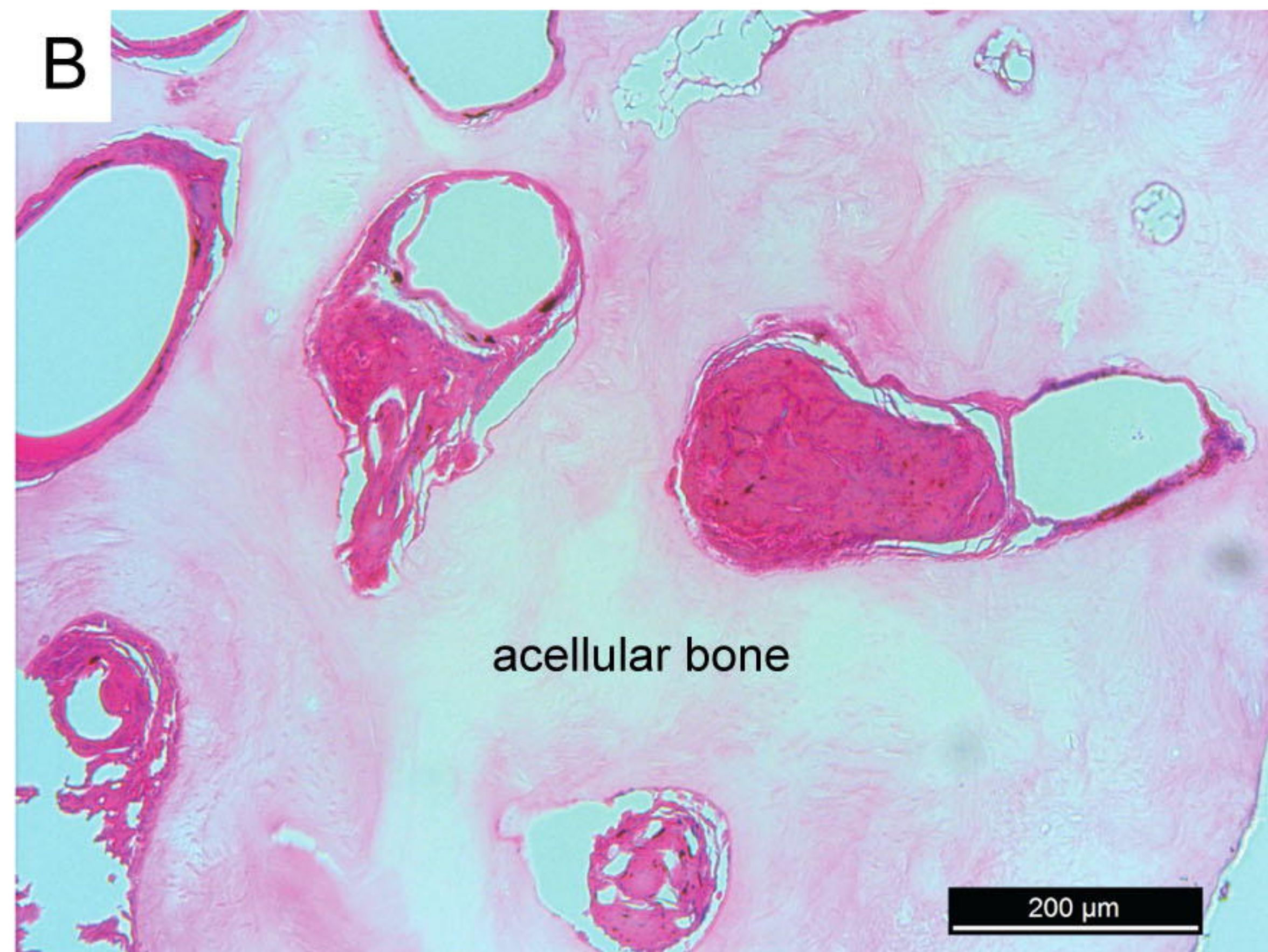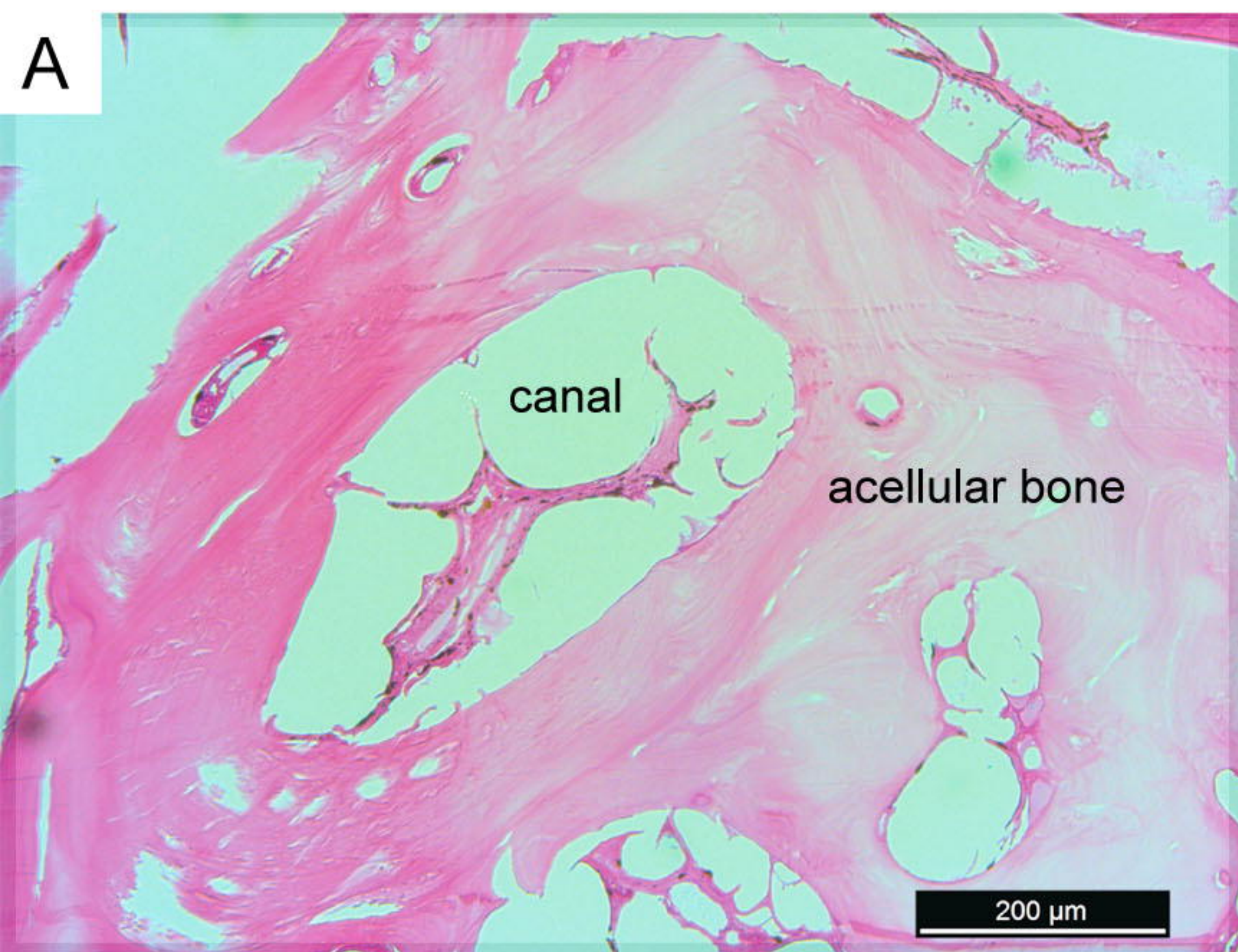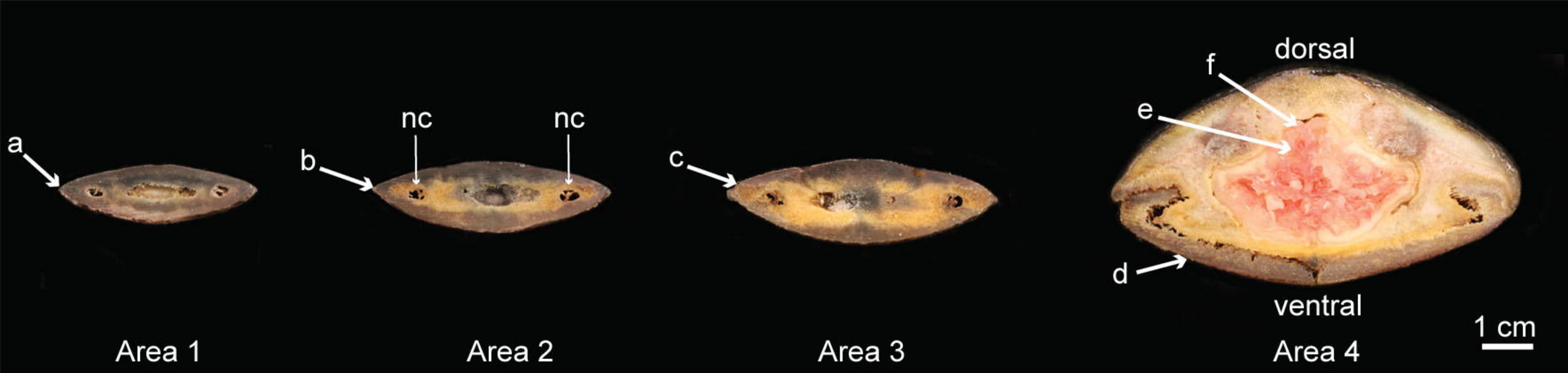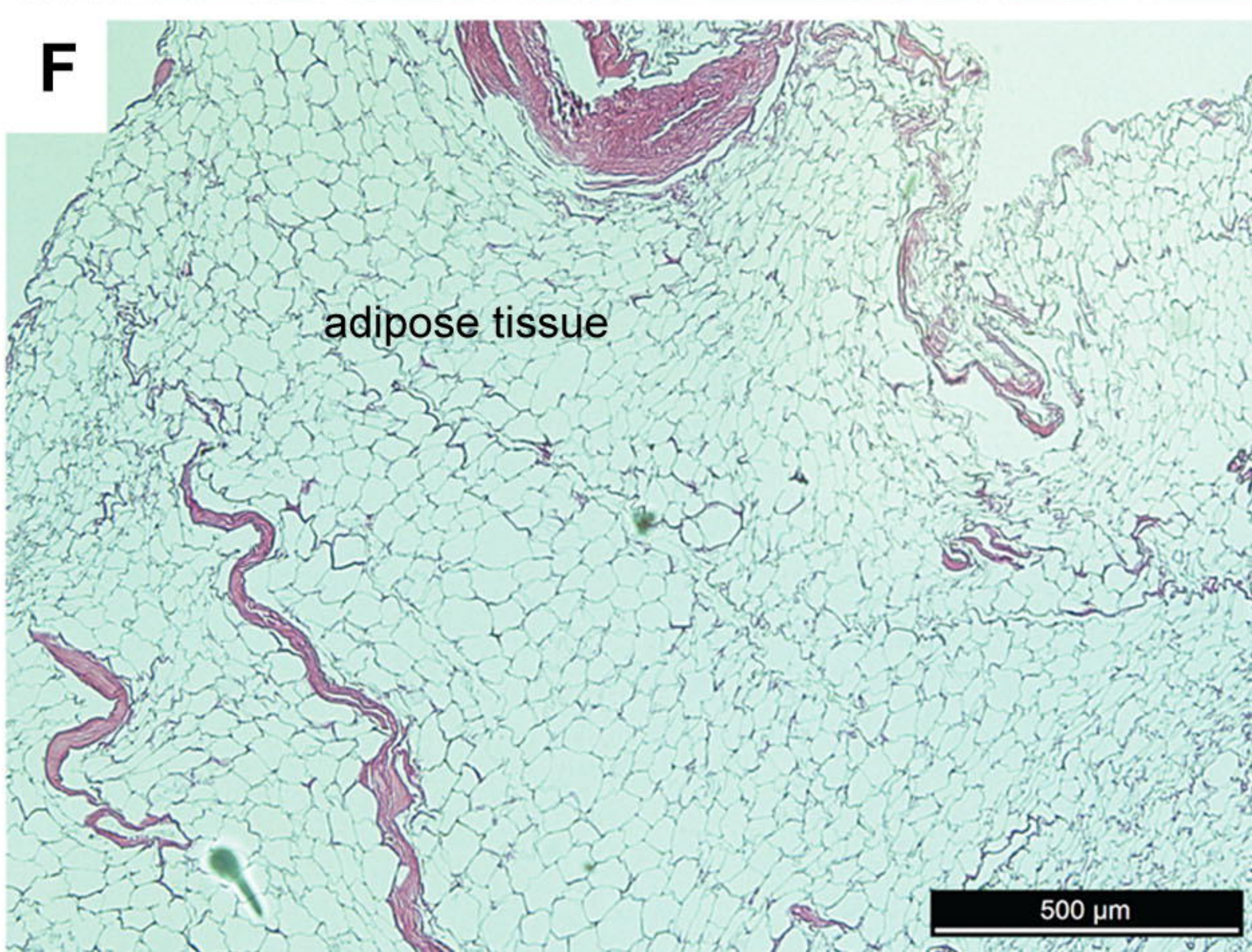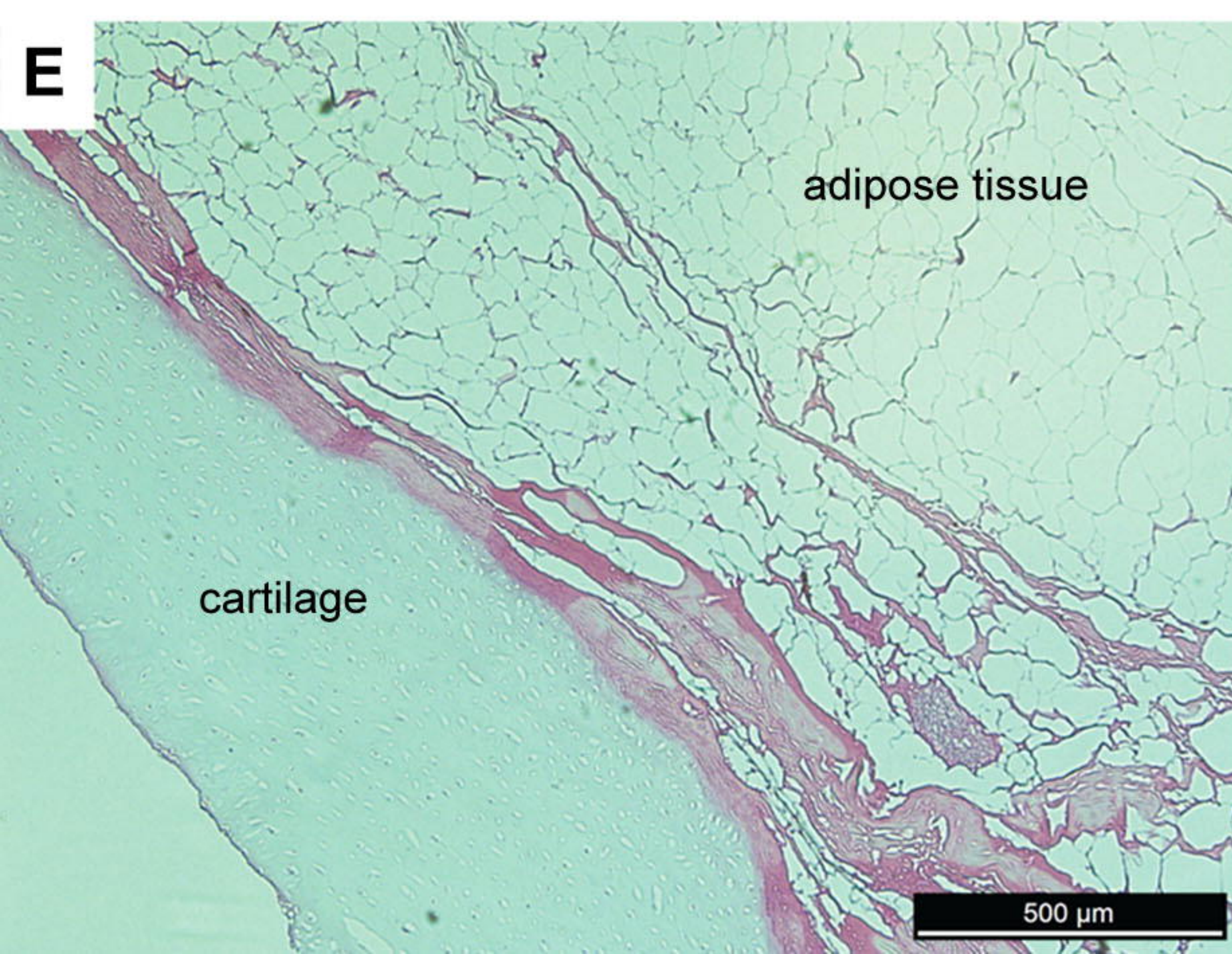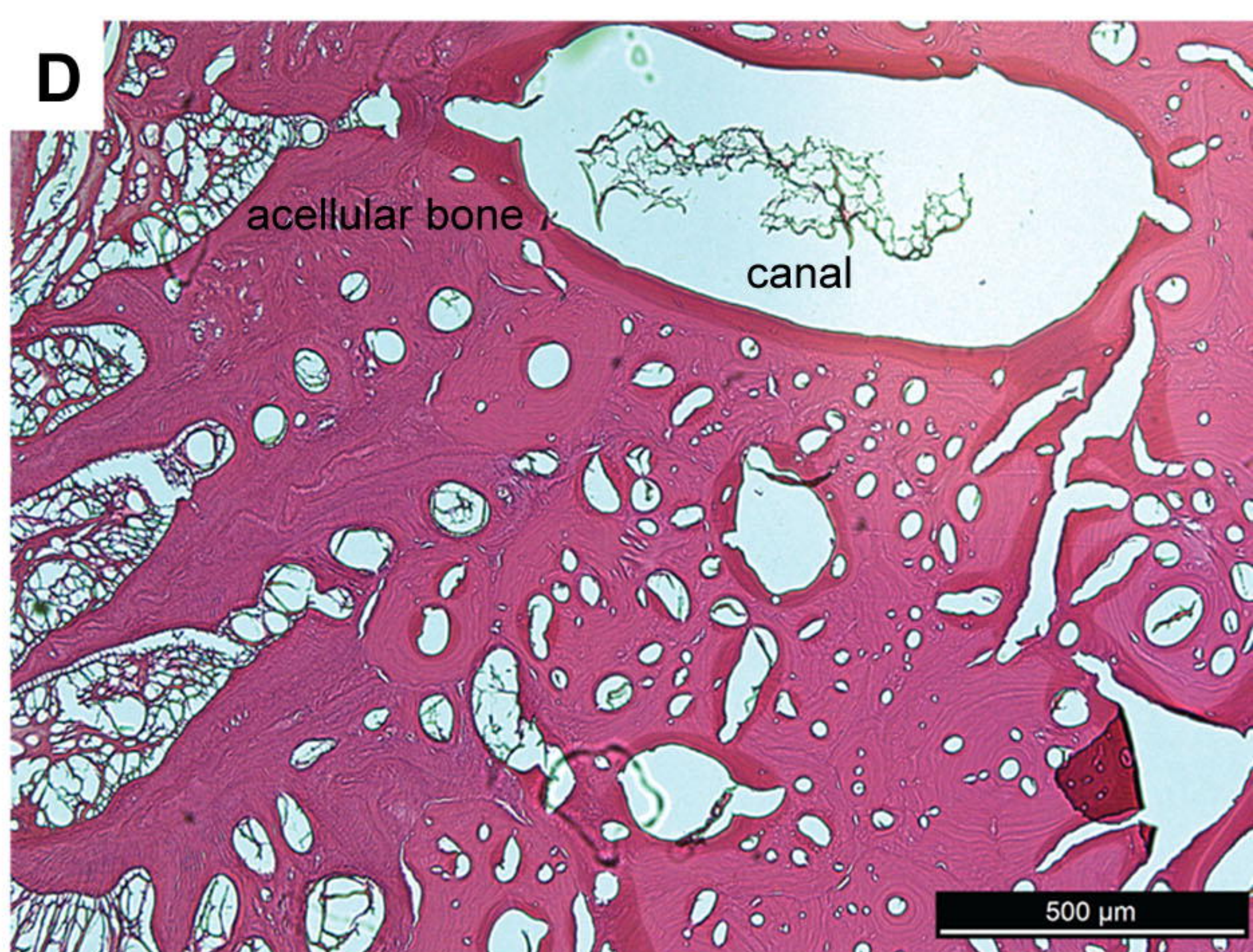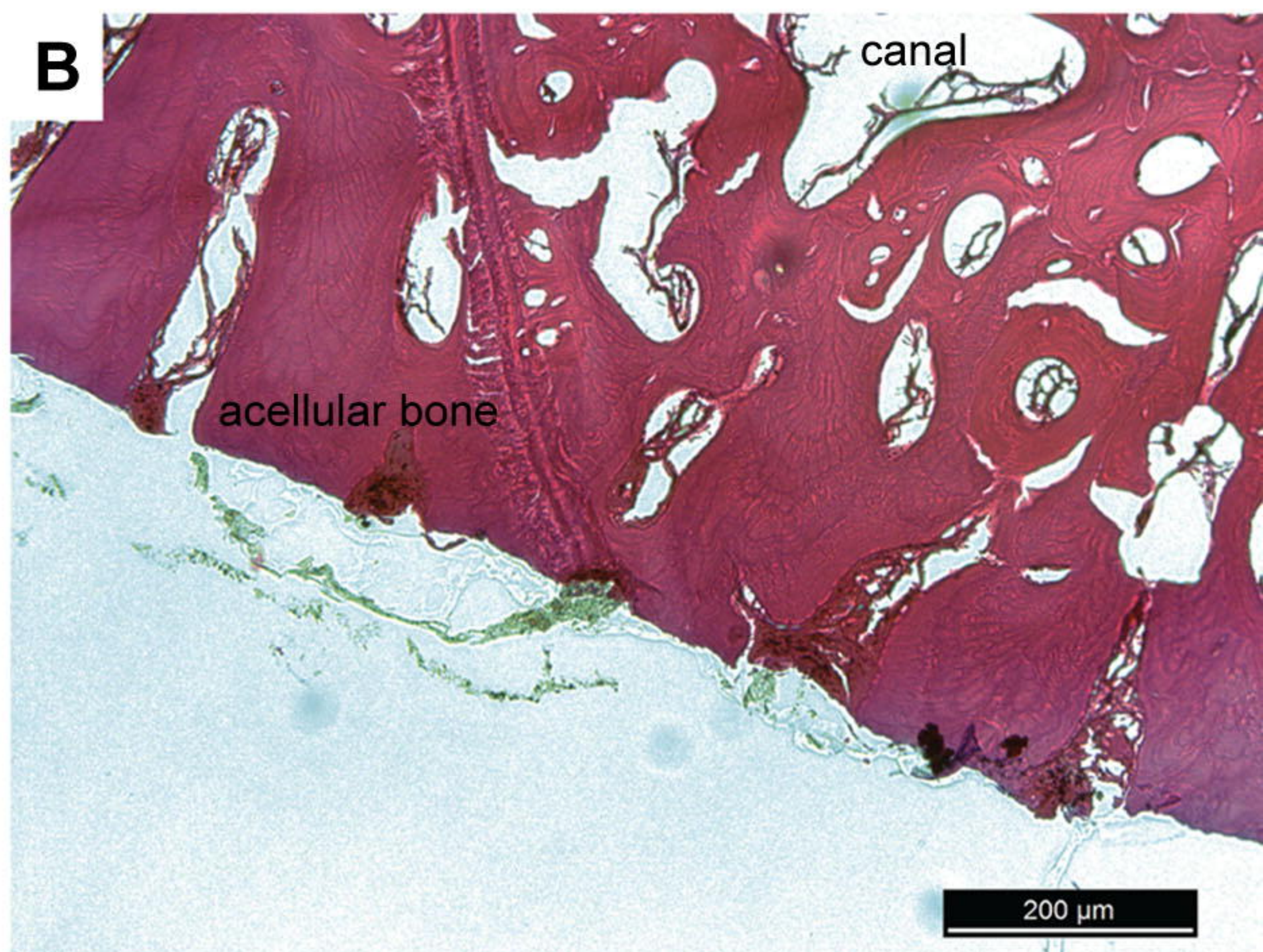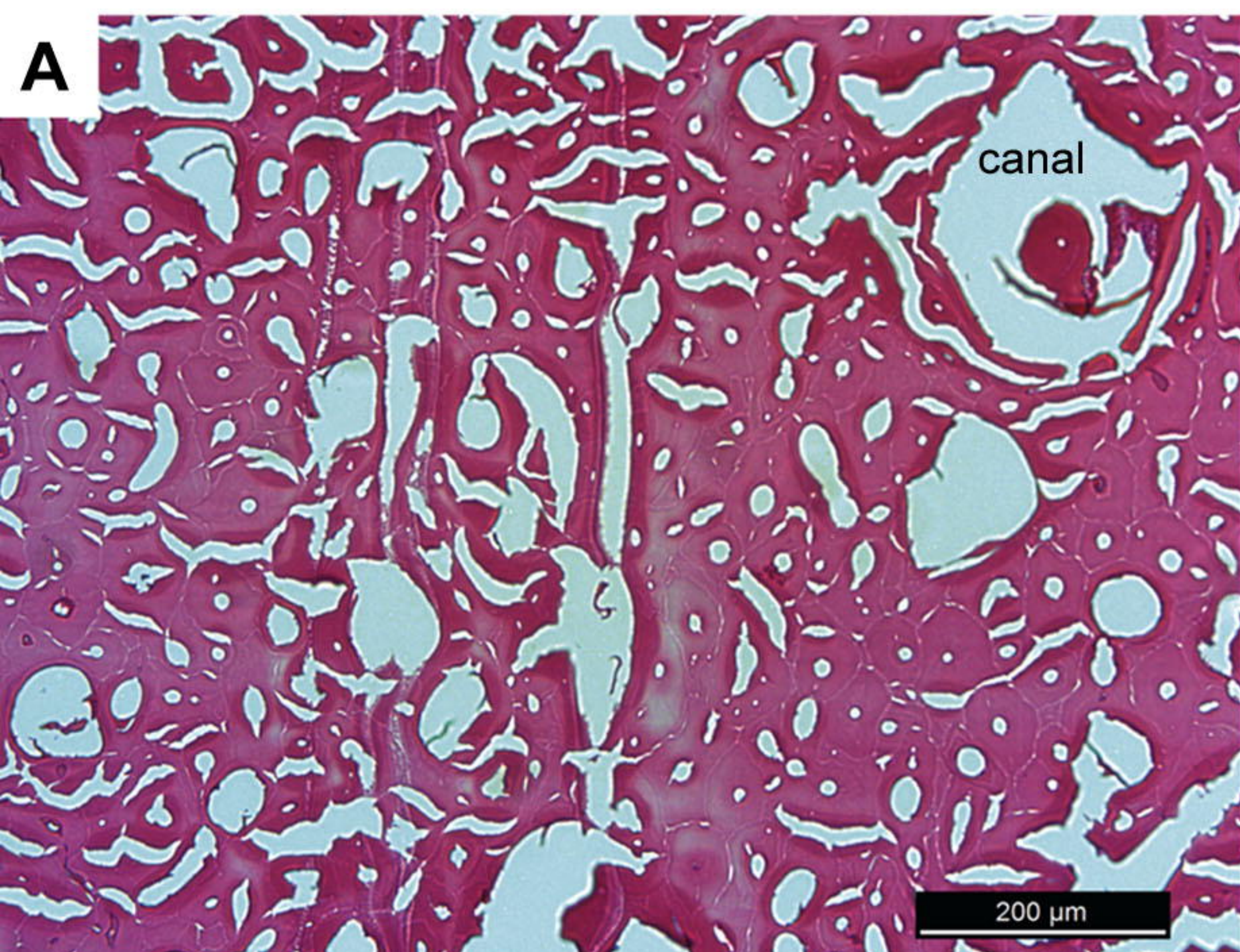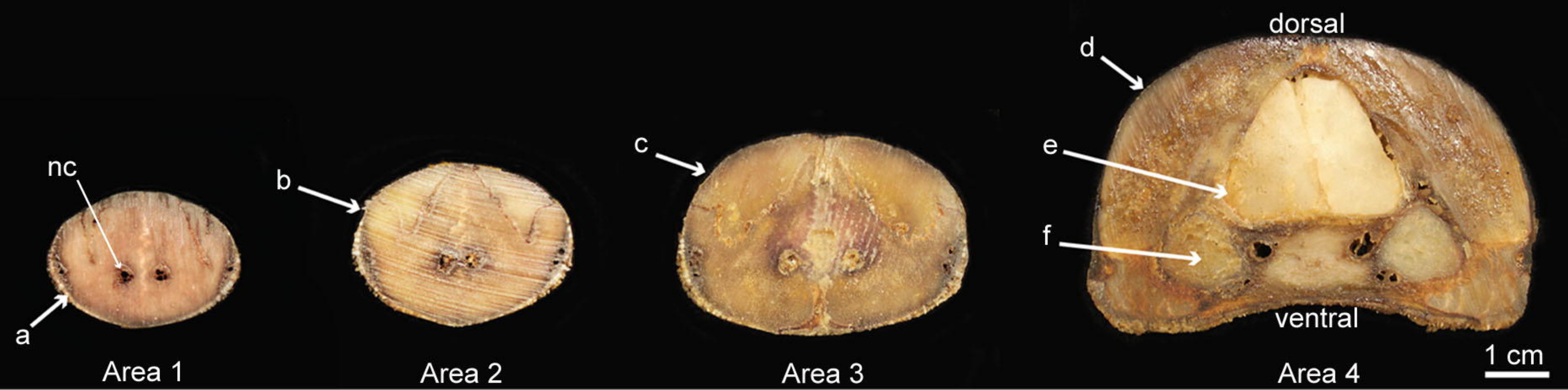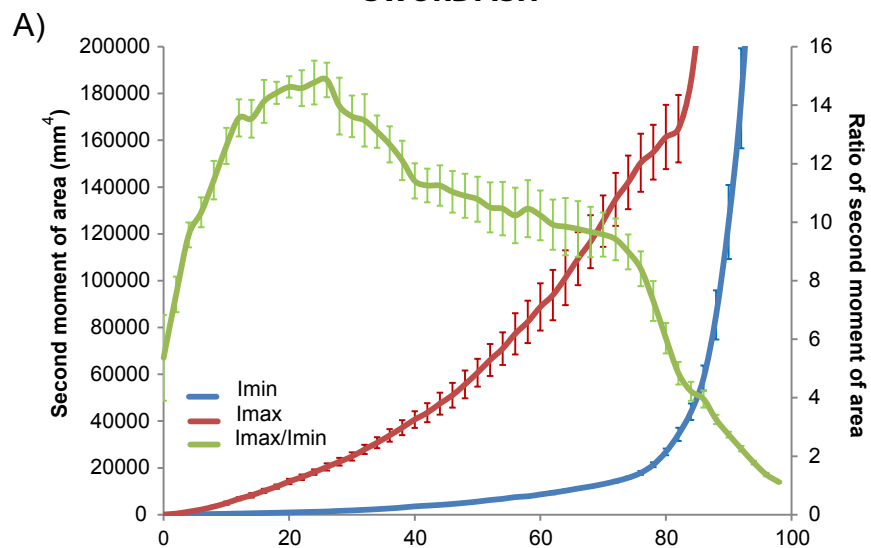
Area 1 Area 2 Area 3 Area 4

A — canal, acellular bone, 200 µm

B — acellular bone, 200 µm

C — acellular bone, 200 µm

D — acellular bone, 200 µm

E — cartilage, 500 µm

F — adipose tissue, 500 µm

SWORDFISH

A)

C)

BLUE MARLIN

B)

D)

Lat. load

D-V load

St. Stress (N/mm²)

Area

● Swordfish
○ Blue marlin

A) Stress/Applied force $(N/mm^2)* N^{-1}$

B) Max Stress (N/mm^2)

C) Drag (N/m)

SWF Lat load
SWF DV load
BM Lat load
BM DV load

Length of rostra (cm)

Swordfish

Blue marlin

0%   100%   0%   100%

MTS

Area 4

Area 3

Area 2

Area 1

d

strain gauges

loading point

holding device

Area 2 cross section

SG

dorsal

o

y

o

NA

ventral
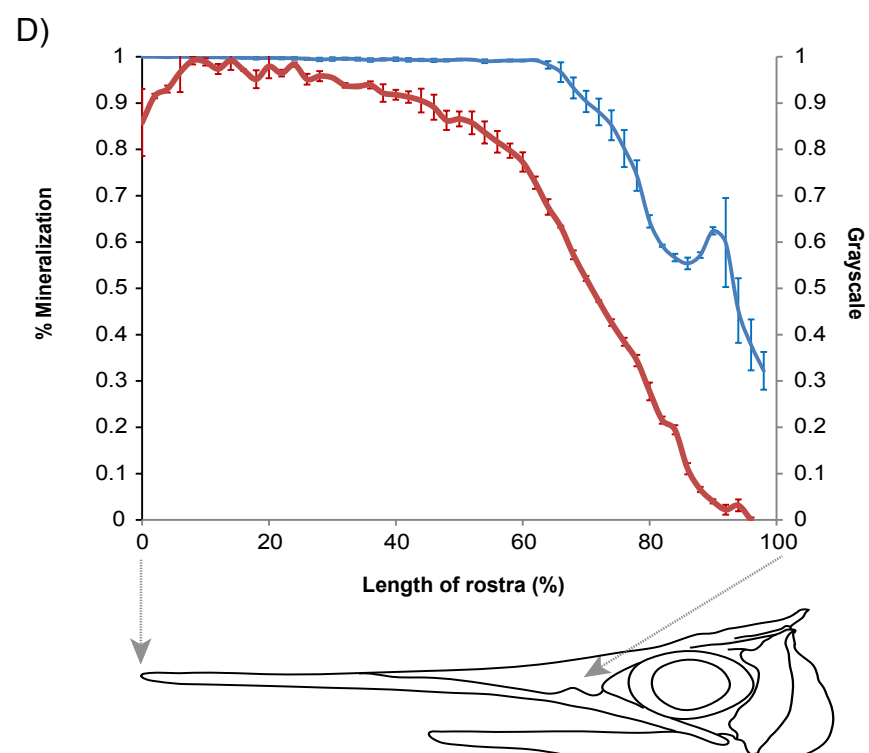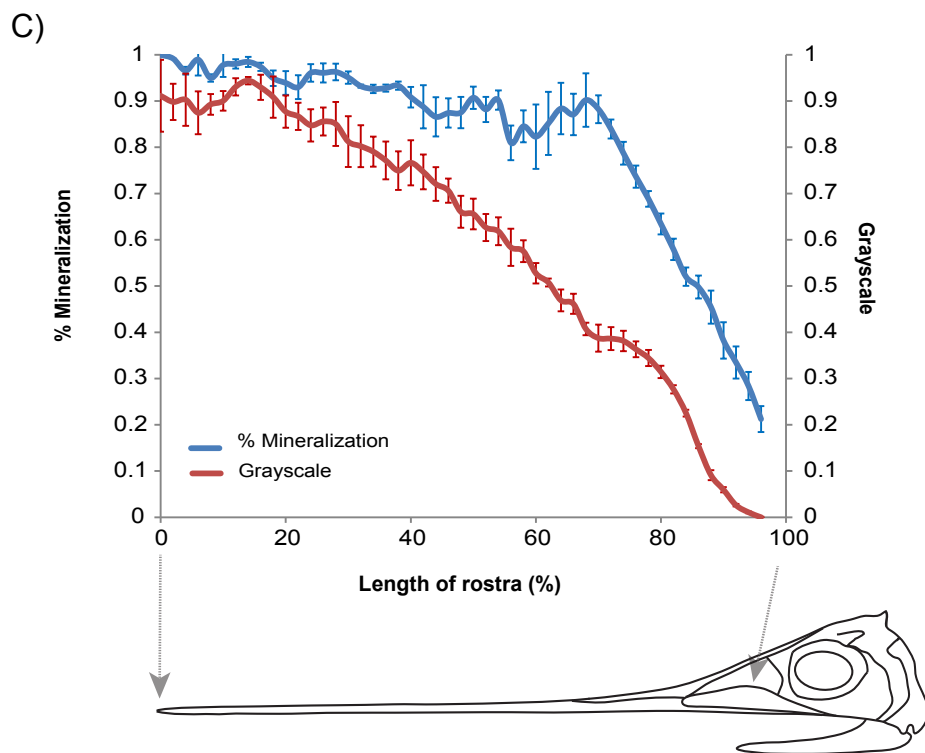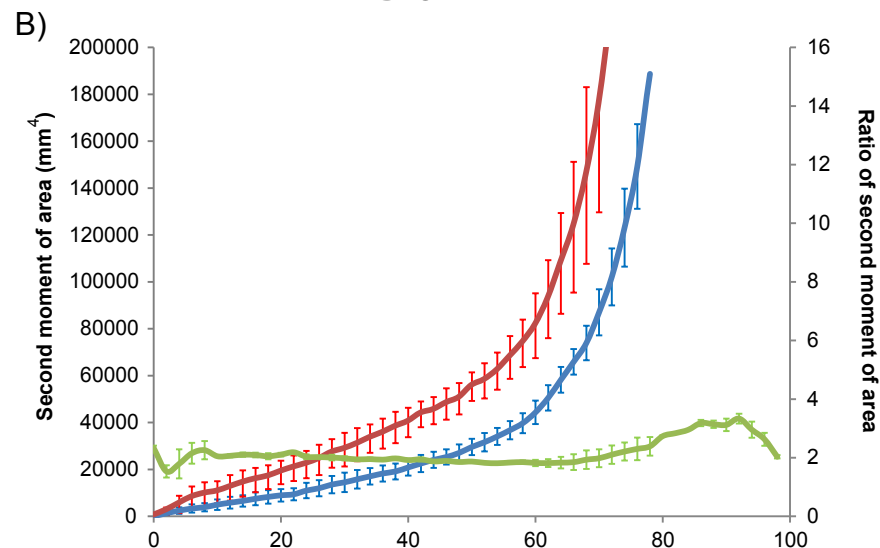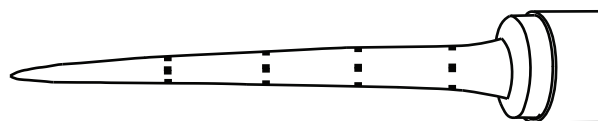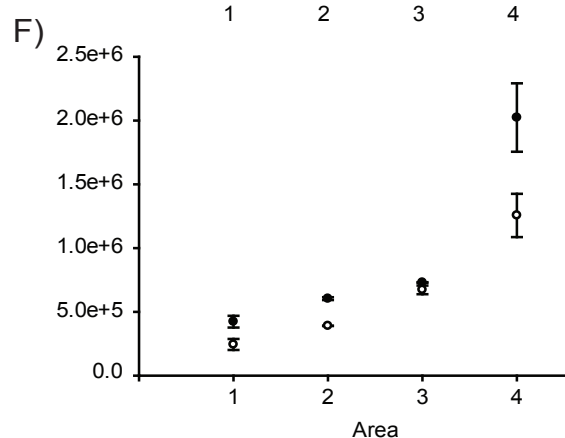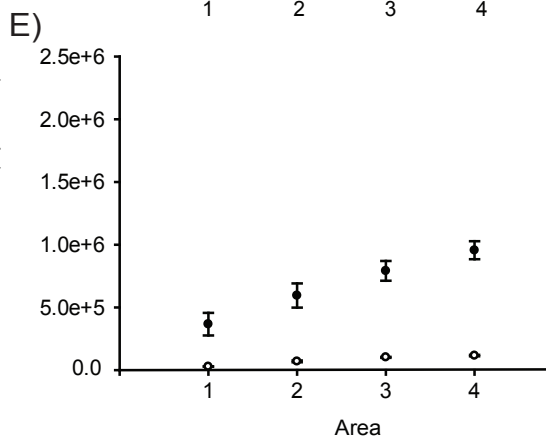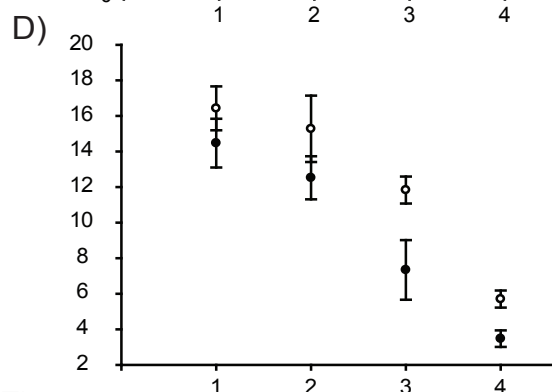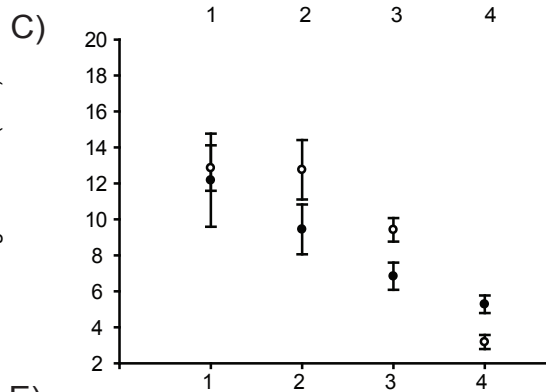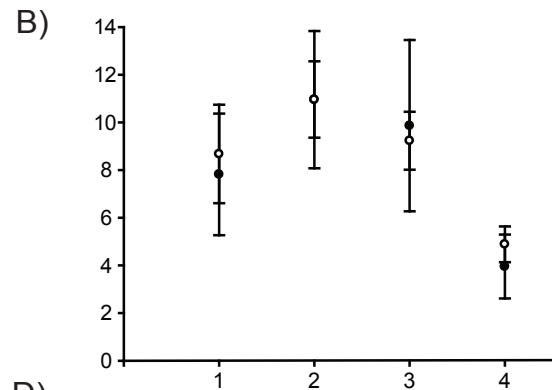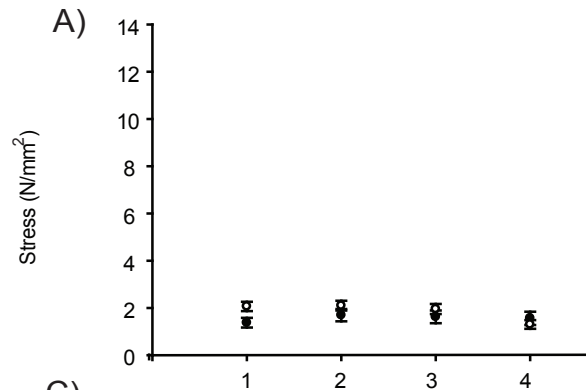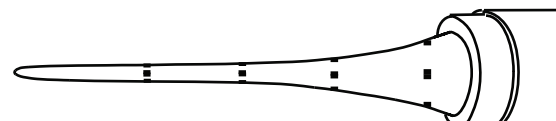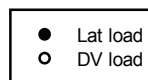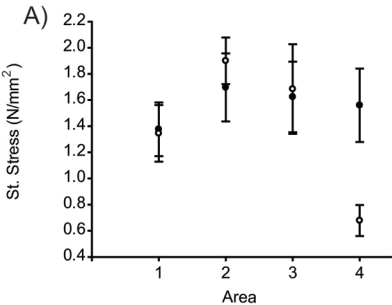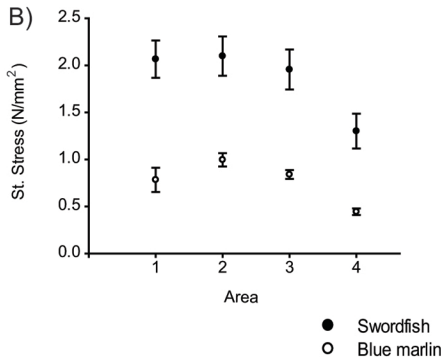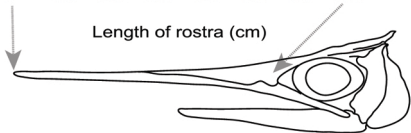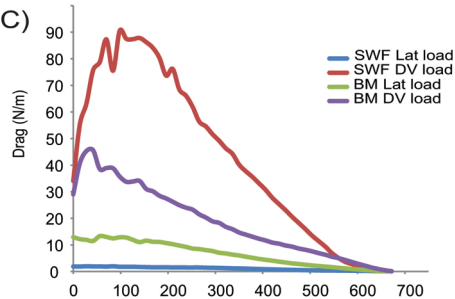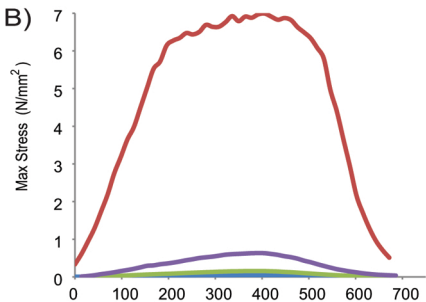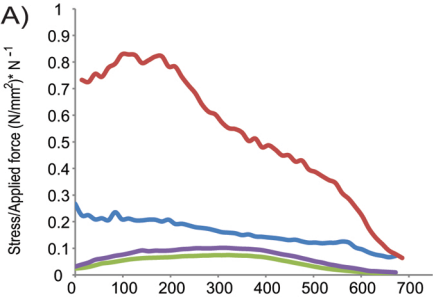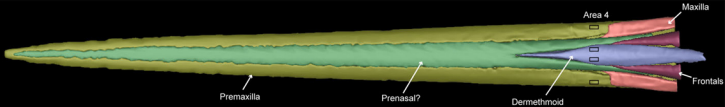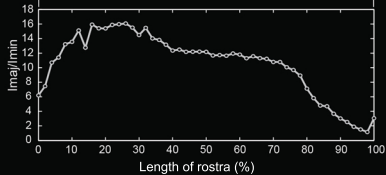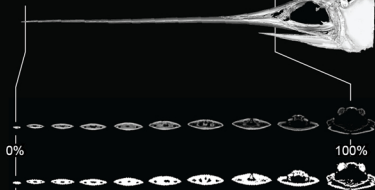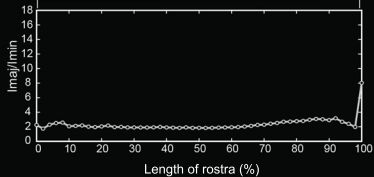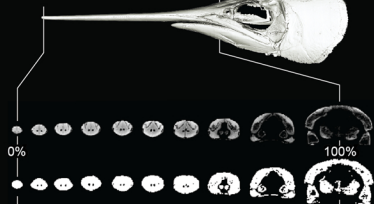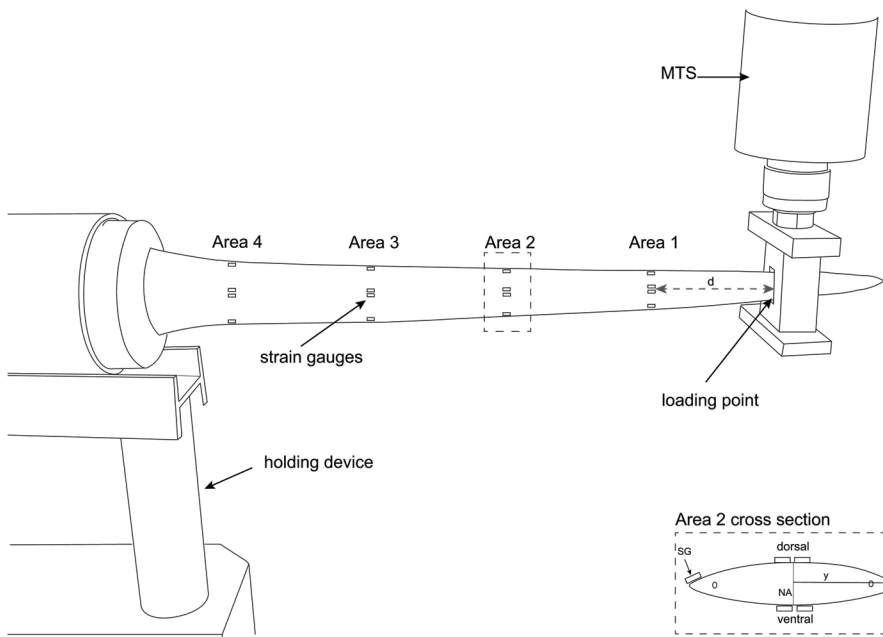
A   **POINT LOADING**

B   **HYDRODYNAMIC LOADING**